Received ; | Revised ; | Accepted

DOI: xxx/xxxx

RESEARCH ARTICLE

Trajectory tracking control based on prescribed performance and fractional-order state observer for unmanned helicopters with unmeasurable states

Shuyi Shao[1,2] | Liwen Wang[1] | Qijun Zhao[2] | Hongtian Chen[3]

[1]College of Automation Engineering, Nanjing University of Aeronautics and Astronautics, Nanjing, China
[2]College of Aerospace Engineering, Nanjing University of Aeronautics and Astronautics, Nanjing, China
[3]Department of Chemicaland Materials Engineering, University of Alberta, Edmonton, Canada

Correspondence
*Shuyi Shao, College of Automation Engineering, Nanjing University of Aeronautics and Astronautics, Nanjing, China. Email: shaosy@nuaa.edu.cn

Funding information
National Natural Science Foundation of China, Grant/Award Number: 62003163; Jiangsu Province Science Foundation for Youths, Grant/Award Number: BK20200415; Jiangsu Province Postdoctoral Science Foundation, Grant/Award Number: 2020Z112; Fundamental Research Funds for the Central Universities, Grant/Award Number: XAC22009

Summary

The tracking control problem of trajectory planning is studied in this paper based on prescribed performance method (PPM) for the small-scale unmanned autonomous helicopter (UAH) with wind-gust disturbances (WGDs) and unmeasurable states. For the purpose, the nonlinear model with flapping dynamics is established, and the transformation performance function is used to ensure that the errors of trajectory tracking satisfy the corresponding performance. The fractional-order observers are investigated to estimate the longitudinal and lateral flapping angles that are treated as unmeasurable states, and estimate the WGDs, respectively. Based on PPM and the designed observers, the fractional-order theory-based backstepping trajectory tracking control scheme is developed for the UAH system, and the three-dimensional trajectory is planned by the improved wolf pack algorithm. Then the stability of the entire system is proven through strict theoretical analysis. Finally, the simulation analysis on the UAH are presented to demonstrate the efficiency of the designed method.

KEYWORDS:
Trajectory tracking control, prescribed performance, fractional-order observer, unmeasurable states

1 | INTRODUCTION

As we all know, unmanned aerial vehicles have been widely used in all aspects of real life, and many types of unmanned aerial vehicles have been designed, and the corresponding flight technologies have been studied. However, as a special kind of aircraft, the unmanned autonomous helicopter (UAH) has many advantages compared with fixed-wing aircrafts, for instance, the hovering in the air, the flying in any direction, the flexible operation, the vertical take-off and landing and so on[1]. Because of the advantages above, the development of UAH has become an important research topic in the aerospace field. Moreover, the UAH has also been widely used in the areas of detection, strike, tracking, target interception, atmospheric monitoring, power monitoring and other military and civilian fields[2]. However, unlike other mechanical systems, the UAH system is an underactuated nonlinear system with multiple-inputs and mutliple-outputs, and its different channels have strong dynamic coupling, which will bring different complex difficulties to the design of flight control methods for UAH systems[3,4]. Therefore, it is very necessary and corresponding engineering application significance to design feasible flight control technologies for the UAH systems.

In general, the linear and nonlinear control methods are two kinds of flight control methods for the UAH systems in the published works. For the linear control methods, for instance, the traditional PID control[5], the H_∞ control[6], the linear active disturbance rejection control[7] and the linear quadratic regulator control[8], etc. But the linear control methods used in the UAH control can only describe the helicopter operation state near the balance point. However, as a nonlinear UAH system with strong coupling, some nonlinear control methods are explored to achieve the effective control of UAH system, for instance, the sliding model control[9], the backstepping control[10,11], the intelligent control based on the neural network[12] and the fuzzy control[13]. For the control methods mentioned above, the backstepping control is heavily applied in the nonlinear control because of its unique design process[14,15]. Furthermore, the backstepping control has been used to investigate and research the trajectory tracking control (TTC) of the various UAHs for its good flexibility and scalability. For instance, in[16], the generalized PI observer and the backstepping control were integrated to come up with a feedforward-feedback compound control scheme. A compound control approach was explored by the synthesis of harmonic disturbance observer and the backstepping control for the tracking control of UAH in[17]. In[18], the backstepping control was employed to inquire into an adaptive anti-disturbance fault-tolerant control scheme for the UAH model subject to actuator fault. In the case of external disturbances, the backstepping control, the sliding model control and the robust anti-disturbance control method were combined and applied to different sub-loops to ensure the stability for the uncertain quadrotor system in[19]. Although the research results have designed nonlinear control technologies for UAH systems, there are still few TTC methods based on the fractional-order theory for UAH systems under wind-gust disturbances (WGDs). Therefore, to improve the robustness of the UAH systems, this kind of control problems may warrant further study.

The WGDs are also a key factor for the outdoor applications of UAHs, especially when the UAHs perform missions in the urban, the valley and the marine environments. If the external WGDs are not considered, it will cause turbulence and thrust fluctuation during the UAH flight, and the stability of the UAH system in the corresponding environment is affected. Thus, the flight quality will be reduced, and even cause the flight safety can not be ensured[20]. Therefore, how to ensure the UAV system has excellent stability performance and the ability to resist external disturbances are the key points for the research of UAH control. In order to have good TTC performance for the UAH under the WGDs, the influence of the rotor flapping motion can not be ignored for the design of the UAH flight control. In[21–23], for the process of designing the UAH tracking controllers, the works either ignored the influence of the rotor flapping motion, or treated the longitudinal and lateral flapping angles (LLFAs) generated by the rotor flapping dynamics as measurable states. However, in the actual flight, it is unrealistic to measure the LLFAs by sensors. Since the state observers can estimate the unknown states effectively, and some control methods based on the state observers have been reported[24–29]. Thus, according to the design methods of the state observer mentioned above, the unknown state estimation of the UAH and the suppression method of WGDs can be studied. Furthermore, on the basis of the advantages of fractional-order control[30], the adjustment margin of the fractional-order controllers and observers designed can be increased accordingly. Therefore, in the field of the UAH control research, designing a reasonable observer by taking advantage of the fractional-order theory to observe the unknown LLFAs is a key problem worth studying for the control of UAH systems.

In addition, in the previous studies on the control schemes of UAH systems, few studies were reported on the combination of the trajectory planning and the UAH systems control. However, in view of the complex flying environment of the UAHs, planning the flight path in advance is helpful to improve the flight safety of UAHs. Further, the effective control methods are adopted to ensure the flight of the UAHs along the planned trajectory and improve the efficiency of the UAHs' mission execution. By reason of the foregoing, the overall works of this paper are : (i) For the safe flight of the UAH in dynamic environments, a three-dimensional trajectory is planned by the improved wolf pack algorithm (WPA), and some traditional trajectory planning algorithms are introduced to compare and show that the improved WPA has better trajectory planning effect; (ii) Aiming at the issues of the WGDs and the unmeasurable LLFAs in the actual flight of the UAH, the LLFAs are taken as the unmeasurable states, and a fractional-order observer is designed to assess the unknown states, and the fractional-order extended state observer (ESO) is developed to tackle the impact of the WGDs; (iii) Considering that the UAH needs to meet the specified performance requirements in the flight process, based on the error transformation function, a backstepping TTC scheme is designed for the UAH system under the performance constraint and the WGDs, and the control scheme can assure that all signals are bounded in the entire system, and the tracking error of the planned trajectory can satisfy the performance of the corresponding design under the developed method.

In the rest of this paper, the organizational structure is presented as follows: the small-scale UAH model under the external WGDs is established in Section 2, and the error transformation function under the prescribed performance method (PPM) is given. In Section 3, the design process of fractional-order observer and ESO are described. In Section 4, the detailed analysis processes of the TTC scheme for the UAH are given, and the stability of the entire system is proven. The simulation anslysis

results and the generation of three-dimensional trajectory tracking are introduced in Section 5, and the corresponding conclusions are given in Section 6.

2 | PROBLEM FORMULATION AND PREPARATION

2.1 | Model Analysis of Unmanned Helicopters

To facilitate analyze the motion characteristics of the UAH, the reference frames are defined as follows: the inertial frame is set as $\mathfrak{R}_e = \{O_e, X_e, Y_e, Z_e\}$, which the centre O_e is usually located at a certain point. The aircraft-body frame is set as $\mathfrak{R}_b = \{O_b, X_b, Y_b, Z_b\}$, which the center O_b is situated at center of the gravity for the UAH. The relationship between the two coordinate frames is shown in Fig. 1 , where the paremeters a and b respectively represent the LLFAs of the main rotor, the variables T_{mr} and Q_{mr} represent the thrust and the main rotor's counter torque, respectively.

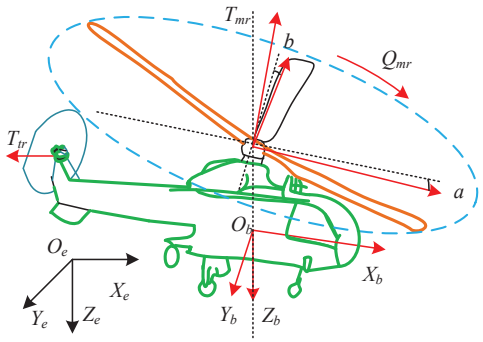

FIGURE 1 Coordinate frames of the unmanned helicopter.

For the actual flight of the UAH, the states such as speed and attitude, will be inevitably influenced by the external WGDs. For the analysis of this paper, the wind-gust in form '1-cos' is used to represent the external wind disturbance suffered by the UAH. The specific mathematical expression of the wind gust model can be described as in[31]

$$\mathcal{V}_{\mathcal{P}} = \begin{bmatrix} \mathcal{V}_{\mathcal{P}x} \\ \mathcal{V}_{\mathcal{P}y} \\ \mathcal{V}_{\mathcal{P}z} \end{bmatrix} = \begin{bmatrix} \frac{\mathcal{V}_{\mathcal{P}xm}}{2}(1 - \cos\frac{\pi x}{d_{\mathcal{P}x}}) \\ \frac{\mathcal{V}_{\mathcal{P}ym}}{2}(1 - \cos\frac{\pi y}{d_{\mathcal{P}y}}) \\ \frac{\mathcal{V}_{\mathcal{P}zm}}{2}(1 - \cos\frac{\pi z}{d_{\mathcal{P}z}}) \end{bmatrix} \tag{1}$$

where $\mathcal{V}_{\mathcal{P}} = [\mathcal{V}_{\mathcal{P}x}, \mathcal{V}_{\mathcal{P}y}, \mathcal{V}_{\mathcal{P}z}]^{\mathrm{T}}$ denotes the corresponding three-axis velocity of the wind-gust in the inertial frames $\mathfrak{R}_e$, $\mathcal{V}_{\mathcal{P}im}, i = x, y, z$ denote the three-axis intensity of the wind-gust, $d_{\mathcal{P}i}, i = x, y, z$ denote the wind-gust scale, and x, y and z respectively denotes the position coordinate of the UAH in the inertial frames.

According to the aerodynamics, the flight dynamic and the external WGDs, the nonlinear model of the UAH is written as[32,33]

$$\begin{aligned} \dot{\mathcal{P}} &= \mathcal{V} + D_{\mathcal{P}} \\ \dot{\mathcal{V}} &= R_b^e F/m + g\vartheta + D_{\mathcal{V}} \\ \dot{\Lambda} &= \mathcal{H}\Omega \\ \dot{\Omega} &= -\mathcal{J}^{-1}(\Omega \times \mathcal{J}\Omega) + \mathcal{J}^{-1}\Sigma + D_{\Omega} \\ \dot{a} &= -a/\tau_e - q + \mathcal{A}_{lon}/\tau_e T_a \\ \dot{b} &= -b/\tau_e - p + \mathcal{B}_{lat}/\tau_e T_b \end{aligned} \tag{2}$$

where $\mathcal{P} = [x, y, z]^{\mathrm{T}}$ is the position of UAH defined in $\mathfrak{R}_e$, $\mathcal{V} = [u, v, w]^{\mathrm{T}}$ is the velocity defined in $\mathfrak{R}_b$, $D_{\mathcal{P}} = \mathcal{V}_{\mathcal{P}} = [d_x, d_y, d_z]^{\mathrm{T}}$, $D_{\mathcal{V}} = [d_u, d_v, d_w]^{\mathrm{T}}$, represents the additional velocity vector caused by the wind-gust, m is the mass, g is the gravity, $\vartheta = [0, 0, 1]^{\mathrm{T}}$, $D_{\Omega} = \mathcal{J}^{-1}R_b^e\Sigma_{\mathcal{P}}$ can be obtained based on the analysis in[34], $\Sigma_{\mathcal{P}}$ represents the additional disturbance torque of the

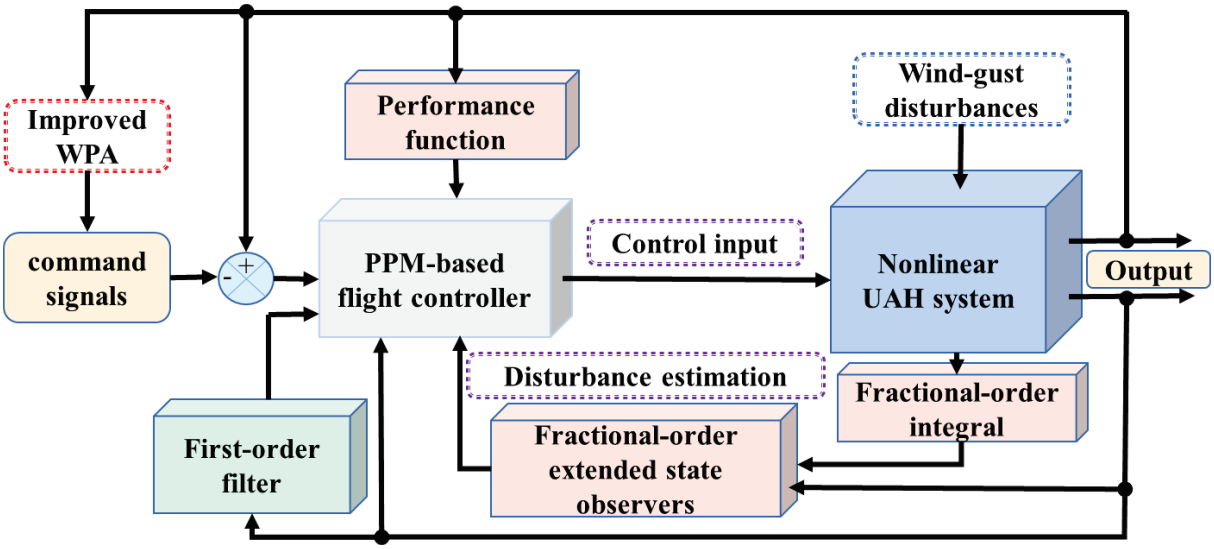

FIGURE 2 The block diagram of the proposed control scheme.

fuselage for the UAH caused by the wind-gust[31], $\Lambda = [\phi, \theta, \psi]^{\mathrm{T}}$ represents the attitude angles, $\Omega = [p, q, r]^{\mathrm{T}}$ represents the attitude angular rates, $\mathcal{J} = \mathrm{diag}\{\mathcal{J}_{xx}, \mathcal{J}_{yy}, \mathcal{J}_{zz}\}$ is the diagonal inertial matrix of UAH, τ_e is the rotor dynamic time constant, $\mathcal{A}_{lon}$ is the longitudinal gain and $\mathcal{B}_{lat}$ is the lateral gain. T_a and T_b are the control inputs. R_b^e and $\mathcal{H}$ represent the transformation matrix from $\mathfrak{R}_b$ to $\mathfrak{R}_e$ and attitude rotation matrix, , respectively. $F = [0, 0, T_{mr}]^{\mathrm{T}}$ and Σ represent the applied resultant force and resultant moment, respectively. Specifically, R_b^e, $\mathcal{H}$ and Σ are described in[35].

In order to promote the tracking controller design, some assumpations and a lemma that need to be used are given as follows, and an overall study block diagram of the corresponding control scheme is presented in Fig. 2 .

Assumption 1. [12] To guarantee that the attitude rotation matrix $\mathcal{H}$ is non-singularity, it can be assumed that $\phi(t) < \left|\frac{\pi}{2}\right|$ and $\theta(t) < \left|\frac{\pi}{2}\right|$ while $t \geq 0$.

Assumption 2. The wind-gust changes uniformly. For the bounded disturbances caused by the wind-gust $D_{\mathcal{P}}$, $D_{\mathcal{V}}$ and D_{Ω} in system (2), the first derivatives are norm bounded.

Assumption 3. The all states in system (2) are measurable except for the LLFAs a and b. Furthermore, the desired position signal $\mathcal{P}_d = [x_d, y_d, z_d]^{\mathrm{T}}$, the yaw angle signal ψ_d and their derivatives $\dot{\mathcal{P}}_d, \dot{\psi}_d, \ddot{\mathcal{P}}_d, \ddot{\psi}_d$ are bounded, that is, there exist unknown positive constants $\Upsilon_{\mathcal{P}}$ and Υ_{ψ} satisfy that $M_{\mathcal{P}} = \{(\mathcal{P}_d, \dot{\mathcal{P}}_d, \ddot{\mathcal{P}}_d) : \mathcal{P}_d^2 + \dot{\mathcal{P}}_d^2 + \ddot{\mathcal{P}}_d^2 \leq \Upsilon_{\mathcal{P}}\}$ and $M_{\psi} = \{(\psi_d, \dot{\psi}_d, \ddot{\psi}_d) : \psi_d^2 + \dot{\psi}_d^2 + \ddot{\psi}_d^2 \leq \Upsilon_{\psi}\}$.

Lemma 1. [36] Under bounded initial conditions at time zero, if one has that the Lyapunov fnction $\bar{V}(x)$ satisfies $\bar{\pi}_1(\|x\|) \leq \bar{V}(x) \leq \bar{\pi}_2(\|x\|)$ and $\dot{\bar{V}}_x \leq -\kappa \bar{V}(x) + M$, where $\bar{\pi}_1, \bar{\pi}_2 : \mathbb{R}^n \to \mathbb{R}$ is a kind of function of $\mathcal{K}^{\infty}$, and κ, M are positive constants, then the variable $x(t)$ is uniformly bounded.

Lemma 2. [37] For the integrable function $\mathcal{F}(t)$, if we have that $\mathcal{F}(t^*)$ for $t^* \in (0, t)$, then one has that $I^{-\mu} |\mathcal{F}(t)| \geq \bar{L}$, where $I^{-\mu}(\bullet)$ is the fractional integral, μ is fractional order, and $\bar{L}$ is a positive constant.

2.2 | Prescribed Performance

During the process of trajectory tracking control for the UAH, it is almost impossible to make the tracking errors converge to zero immediately, but the overshoot is likely to reach to a high value, which may increase the risk of uncontrollable aircraft. To improve this problem, a feasible prescribed performance control strategy is adopted to restrict the tracking errors to ensure that the system achieves satisfactory transient and steady-state performance (TSSP). Firstly, defining the tracking error fo the position, one has that $e_{\mathcal{P}} = \mathcal{P}_d - \mathcal{P} = [e_x, e_y, e_z]^{\mathrm{T}} = [e_{y1}, e_{y2}, e_{y3}]^{\mathrm{T}}$ and the yaw tracking error $e_{\psi} = \psi_d - \psi = e_{y4}$, where $\mathcal{P} = [x, y, z]^{\mathrm{T}}$, $\mathcal{P}_d = [x_d, y_d, z_d]^{\mathrm{T}}$ is the desired position vector and ψ_d is the desired yaw angle vector. On the basis of the PPM, the tracking error $e_y = [e_{y1}, e_{y2}, e_{y3}, e_{y4}]^{\mathrm{T}}$ is strictly limited to a predefined region by the time attenuation function. The

specific form is written as[38]

$$-\lambda_{1i}\bar{\rho}_i(t) < e_{\mathcal{Y}i}(t) < \lambda_{2i}\bar{\rho}_i(t), i = 1, 2, 3, 4 \tag{3}$$

where $\lambda_{1i} \in (0, 1]$ and $\lambda_{2i} \in (0, 1]$ are paremeters to be designed, $\bar{\rho}_i(t)$ denotes the prescribed performance function, which can be described as[38]

$$\bar{\rho}_i(t) = (\bar{\rho}_{i0} - \bar{\rho}_{i\infty})e^{-\sigma_i t} + \bar{\rho}_{i\infty} \tag{4}$$

where $\bar{\rho}_{i0} > 0$ is an initial value of $\bar{\rho}_i(t)$, $\lim_{t\to\infty} = \bar{\rho}_{i\infty} > 0$, $\sigma_i > 0$ denotes the positive constant. Meanwhile, one has that $\bar{\rho}_i(t)$ is a smooth decreasing function and satisfies that $-\lambda_{1i}\bar{\rho}_{10} < e_{\mathcal{Y}i}(0) < \lambda_{2i}\bar{\rho}_{10}, i = 1, 2, 3, 4$. Furthermore, according to the results in[38], the following transformed error variable β_i is written as

$$\beta_i = Q(\frac{e_{\mathcal{Y}i}(t)}{\bar{\rho}_i(t)}) \tag{5}$$

where $Q(\cdot) : (-\lambda_{1i}, \lambda_{2i}) \to (-\infty, \infty)$ is a strictly increasing smooth function. Therefore, the corresponding transformed error variable β_i is utilized to ensure that the system (2) achieves better performance. Hence, the control target of the system can be transformed into designing a reasonable controller so that the transformed variable β_i is bounded. So, the transformed function is choosen as

$$Q(\frac{e_{\mathcal{Y}i}(t)}{\bar{\rho}_i(t)}) = (1 - \alpha(\frac{e_{\mathcal{Y}i}(0)}{\bar{\rho}_i(0)}))\frac{e_{\mathcal{Y}i}(t)/\bar{\rho}_i(t)}{\lambda_{1i} + e_{\mathcal{Y}i}(t)/\bar{\rho}_i(t)} + \alpha(\frac{e_{\mathcal{Y}i}(0)}{\bar{\rho}_i(0)})\frac{e_{\mathcal{Y}i}(t)/\bar{\rho}_i(t)}{\lambda_{2i} - e_{\mathcal{Y}i}(t)/\bar{\rho}_i(t)} \tag{6}$$

where $\alpha_i = \alpha(\frac{e_{\mathcal{Y}i}(0)}{\bar{\rho}_i(0)}) = \begin{cases} 1, & e_{\mathcal{Y}i}(0) \geq 0 \\ 0, & e_{\mathcal{Y}i}(0) < 0 \end{cases}$.

Then, one can obtain

$$\dot{\beta}_i = \bar{\rho}_i(t)\Pi_i\dot{e}_{\mathcal{Y}i}(t) - \dot{\bar{\rho}}_i(t)\Pi_i e_{\mathcal{Y}i}(t) \tag{7}$$

where $\Pi_i = (1 - \alpha_i)\frac{\lambda_{1i}}{(\lambda_{1i}\bar{\rho}_i(t)+e_{\mathcal{Y}i}(t))^2} + \alpha_i\frac{\lambda_{2i}}{(\lambda_{2i}\bar{\rho}_i(t)-e_{\mathcal{Y}i}(t))^2}$. Then, defining $\beta = [\beta_x, \beta_y, \beta_z, \beta_\psi]^{\mathrm{T}} = [\beta_1, \beta_2, \beta_3, \beta_4]^{\mathrm{T}}$, $\bar{\rho} = \mathrm{diag}\{\bar{\rho}_x, \bar{\rho}_y, \bar{\rho}_z, \bar{\rho}_\psi\} = \mathrm{diag}\{\bar{\rho}_1, \bar{\rho}_2, \bar{\rho}_3, \bar{\rho}_4\}$, $\Pi = \mathrm{diag}\{\Pi_z, \Pi_y, \Pi_z, \Pi_\psi\} = \mathrm{diag}\{\Pi_1, \Pi_2, \Pi_3, \Pi_4\}^{\mathrm{T}}$, and one has

$$\dot{\beta} = \bar{\rho}\Pi\dot{e}_{\mathcal{Y}} - \dot{\bar{\rho}}\Pi e_{\mathcal{Y}} \tag{8}$$

Remark 1. [38] Consider the error $e_{\mathcal{Y}}$ and the defined transformed error β_i in (5). If β_i can be ensure to be bounded, the prescribed performance of $e_{\mathcal{Y}}(t)$ can be satisfied for all $t \geq 0$, then, the form (3) is satisfied.

On the basis of the description, this paper aims at designing a TTC method with four control inputs $U = [T_{mr}, T_{tr}, T_a, T_b]^{\mathrm{T}}$, so that the output $\mathcal{Y} = [x, y, z, \psi]^{\mathrm{T}}$ can follow the desired yaw angle ψ_d and the desired position of the desired trajectory planned by the improved WPA, and the corresponding error can astricte to the predefined bounds by using PPF.

3 | FLAPPING ANGLES AND DISTURBANCE ESTIMATION

3.1 | Estimation of Flapping Angles

In the actual system, the attitude angle and the corresponding angle rate of the UAH can be measured by the sensors installed on the airframe. But it is unrealistic to measure the flapping angles by installing sensors on the rotor, so this paper considers the LLFAs a and b in the flapping movement of the UAH as unmeasurable states. Considering the dynamic model of the UAH with a and b as follows:

$$\begin{aligned} \dot{\Omega} &= -\mathcal{J}^{-1}(\Omega \times \mathcal{J}\Omega) + \mathcal{J}^{-1}\Sigma + D_\Omega \\ \dot{a} &= -a/\tau_e - q + \mathcal{A}_{lon}/\tau_e T_a \\ \dot{b} &= -b/\tau_e - p + \mathcal{B}_{lat}/\tau_e T_b \end{aligned} \tag{9}$$

Since a and b are unmeasurable state variables, for convenience of the subsequent high-gain observer design, the relevant state variables are redefined. Defining $\varpi_1 = \Omega = [p, q, r]^{\mathrm{T}}$, $\varpi_2 = [a, b]^{\mathrm{T}}$, $u_1 = [T_a, T_b]^{\mathrm{T}}$, then (9) can be rewritten as

$$\begin{aligned} \dot{\varpi}_1 &= f_1 + g_1[\varpi_2^{\mathrm{T}}, T_{tr}]^{\mathrm{T}} + D_\Omega \\ \dot{\varpi}_2 &= f_2 + \bar{g}_2 u_1 \end{aligned} \tag{10}$$

where $f_1 = -\mathcal{J}^{-1}(\Omega \times J\Omega) + \mathcal{J}^{-1}[0, 0, -Q_{mr}]^{\mathrm{T}}$, $g_1 = \mathcal{J}^{-1}\begin{bmatrix} 0 & C_m + T_{mr}L_z & -H_z \\ C_m + T_{mr}L_z & 0 & 0 \\ 0 & 0 & H_x \end{bmatrix}$, $f_2 = \begin{bmatrix} -a/\tau_e - q \\ -b/\tau_e - p \end{bmatrix}$, $\bar{g}_2 = \begin{bmatrix} \mathcal{A}_{lon}/\tau_e & 0 \\ 0 & \mathcal{B}_{lat}/\tau_e \end{bmatrix}$, C_m is the stiffness coefficient of the main rotor, L_z is the relative distance, H_x and H_z are the relative longitudinal distance and the vertical distance, respectively.

From (10), it can be seen that the actual contol input $[T_{tr}, T_a, T_b]^{\mathrm{T}}$ is distributed in different loops, and the UAH system is not the strict form of feedback. To facilitate to subsequent estimation of the flapping angles and the design of the trajectory tracking controller, a reasonable tail rotor actuator dynamics is introduced to solve the problem. Thence, the specific first-order equation[39] is introduced as follows:

$$\frac{T_{tr}}{T_n} = \frac{A_t}{\tau_2 s + 1} \tag{11}$$

where A_t represents the gain of tail rotor total pitch input to the tail rotor thrust, and T_n represents the pitch input.

Redefining $u_f = [T_a, T_b, T_n]^{\mathrm{T}}$, $\varpi_2 = [a, b, T_{tr}]^{\mathrm{T}}$, and according to the (9)-(11), (10) can be rewritten as

$$\begin{aligned} \dot{\varpi}_1 &= f_1 + g_1\varpi_2 + D_\Omega \\ \dot{\varpi}_2 &= \Gamma\varpi_2 + I\varpi_1 + g_2u_f \end{aligned} \tag{12}$$

where $\Gamma = \begin{bmatrix} -1/\tau_e & 0 & 0 \\ 0 & -1/\tau_e & 0 \\ 0 & 0 & -1/\tau_2 \end{bmatrix}$, $I = \begin{bmatrix} 0 & -1 & 0 \\ -1 & 0 & 0 \\ 0 & 0 & 0 \end{bmatrix}$, $g_2 = \begin{bmatrix} \mathcal{A}_{lon}/\tau_e & 0 & 0 \\ 0 & \mathcal{B}_{lat}/\tau_e & 0 \\ 0 & 0 & A_t/\tau_2 \end{bmatrix}$.

According to (12), a fractional-order observer is designed as

$$\begin{aligned} \dot{\hat{\varpi}}_1 &= f_1 + g_1\hat{\varpi}_2 + \hat{D}_\Omega + \alpha_1\tilde{\varpi}_1 + \alpha_0\mathcal{E}_{\varpi_{10}}I_f^{-\upsilon_{\varpi_1}}\mathcal{E}_{\varpi_{11}} + \|g_1\|^2\tilde{\varpi}_1 \\ \dot{\hat{\varpi}}_2 &= \Gamma\hat{\varpi}_2 + I\varpi_1 + g_2u_f + \alpha_2\tilde{\varpi}_1 \end{aligned} \tag{13}$$

where $\tilde{\varpi}_1 = \varpi_1 - \hat{\varpi}_1$, $\hat{\varpi}_1$ and $\hat{\varpi}_2$ are the estimation of ϖ_1 and ϖ_2, respectively. $\alpha_0 \in \Re^{3\times3}$, $\alpha_1 \in \Re^{3\times3}$ and $\alpha_2 \in \Re^{3\times3}$ are the designed diagonal matrices to be designed. $\mathcal{E}_{\varpi_{10}} = [\tilde{\varpi}_1^{\mathrm{T}}, 0_{3\times2}] \in \Re^{3\times3}$. $\mathcal{E}_{\varpi_{11}}$ is the vector for the absolute values of each of the variables in the error $\tilde{\varpi}_1$, and υ_{ϖ_1} is the frational order.

Defining the estimation error $\tilde{\varpi}_2 = \varpi_2 - \hat{\varpi}_2$ and $\tilde{D}_\Omega = \hat{D}_\Omega - D_\Omega$. Derivating $\hat{\varpi}_1$ and $\hat{\varpi}_2$, one can obtain

$$\begin{aligned} \dot{\tilde{\varpi}}_1 &= g_1\tilde{\varpi}_2 - \alpha_1\tilde{\varpi}_1 - \tilde{D}_\Omega - \|g_1\|^2\tilde{\varpi}_1 - \alpha_0\mathcal{E}_{\varpi_{10}}I_f^{-\upsilon_{\varpi_1}}\mathcal{E}_{\varpi_{11}} \\ \dot{\tilde{\varpi}}_2 &= \Gamma\tilde{\varpi}_2 - \alpha_2\tilde{\varpi}_1 \end{aligned} \tag{14}$$

According to (14), the boundedness of observation error $\tilde{\varpi}_1$ and $\tilde{\varpi}_2$ will be proven in the following section. Meanwhile, the model (2) is rewritten as

$$\begin{aligned} \dot{\mathcal{P}} &= \mathcal{V} + D_{\mathcal{P}} \\ \dot{\mathcal{V}} &= R_b^eF/m + g\vartheta + D_{\mathcal{V}} \\ \dot{\Lambda} &= \mathcal{H}\Omega \\ \dot{\varpi}_1 &= f_1 + g_1\varpi_2 + D_\Omega \\ \dot{\varpi}_2 &= \Gamma\varpi_2 + I\varpi_1 + g_2u_f \end{aligned} \tag{15}$$

Remark 2. The real system input is $u = [T_a, T_b, T_{tr}]^{\mathrm{T}}$ for the attitude rate and flapping dynamics subsystem of UAH. Since system model in (15) is not a strict form of feedback so that it is not suitable for applying backstepping method to design the controller. By considering (11), the above problem is solved and the corresponding control input $u_f = [T_a, T_b, T_n]^{\mathrm{T}}$ can be obtained. Meanwhile, the actual input $u = [T_a, T_b, T_{tr}]^{\mathrm{T}}$ can also be obtained through the relevance between T_{tr} and T_n in (11).

3.2 | Fractional-order Extended State Observers

Considering the following unmanned helicopter subsystems with external WGDs:

$$\begin{aligned} \dot{\mathcal{P}} &= \mathcal{V} + D_{\mathcal{P}} \\ \dot{\mathcal{V}} &= R_b^eF/m + g\vartheta + D_{\mathcal{V}} \\ \dot{\varpi}_1 &= f_1 + g_1\varpi_2 + D_\Omega \end{aligned} \tag{16}$$

Since the distance $D_{\mathcal{P}} \in \mathfrak{R}^{3\times3}$, $D_{\mathcal{V}} \in \mathfrak{R}^{3\times3}$ and $D_{\Omega} \in \mathfrak{R}^{3\times3}$ are unknown, the fractional-order ESO is designed to restrain the affect of the external WGDs as follows:

Defining $D_{\mathcal{P}}$, $D_{\mathcal{V}}$ and D_{Ω} as the extended states of the system in (16) and let $\mathcal{P} = x_1$, $\mathcal{V} = x_2$, $D_{\mathcal{P}} = x_3$, $D_{\mathcal{V}} = x_4$, $\varpi_1 = x_5$ and $D_{\Omega} = x_6$. Then the system (16) is rewritten as

$$\begin{aligned} \dot{\bar{x}}_1 &= \mathcal{X}_1 + \bar{x}_2 \\ \dot{\bar{x}}_2 &= h^*(t) \end{aligned} \tag{17}$$

where $\bar{x}_1 = [x_1^{\mathrm{T}}, x_2^{\mathrm{T}}, x_5^{\mathrm{T}}]^{\mathrm{T}}$, $\mathcal{X}_1 = [x_2^{\mathrm{T}}, (R_b^e F/m + g\vartheta)^{\mathrm{T}}, (f_1 + g_1\varpi_2)^{\mathrm{T}}]^{\mathrm{T}}$, $\bar{x}_2 = [x_3^{\mathrm{T}}, x_4^{\mathrm{T}}, x_6^{\mathrm{T}}]^{\mathrm{T}}$, $h^*(t) = [h_1^{*\mathrm{T}}, h_2^{*\mathrm{T}}, h_3^{*\mathrm{T}}]^{\mathrm{T}}$ is a function vector for the bounded time derivatives of the disturbances $D_{\mathcal{P}}$, $D_{\mathcal{V}}$ and D_{Ω}.

Define the errors as $e_1 = \hat{x}_1 - x_1$, $e_2 = \hat{x}_2 - x_2$, $e_3 = \hat{x}_3 - x_3$, $e_4 = \hat{x}_4 - x_4$, $e_5 = \hat{x}_5 - x_5$, and $e_6 = \hat{x}_6 - x_6$. Then the fractional-order ESO is designed as

$$\begin{aligned} \dot{\hat{\bar{x}}}_1 &= \hat{\mathcal{X}}_1 + \hat{\bar{x}}_2 - \bar{\beta}_1\mathcal{E}_1 I_f^{-\upsilon_0}\mathcal{E}_2 - \bar{\beta}_2\bar{e}_1 - \left\|g_1\right\|^2\bar{e}_1 \\ \dot{\hat{\bar{x}}}_2 &= -\bar{\beta}_3\bar{e}_1 - \bar{\beta}_4\hat{\bar{x}}_2 \end{aligned} \tag{18}$$

where $\hat{\bar{x}}_1$ and $\hat{\bar{x}}_2$ represent the estimations of $\bar{x}_1$ and $\bar{x}_2$ respectively. $\hat{x}_3 = \hat{D}_P = [\hat{d}_x, \hat{d}_y, \hat{d}_z]^{\mathrm{T}}$, $\hat{x}_4 = \hat{D}_V = [\hat{d}_u, \hat{d}_v, \hat{d}_w]^{\mathrm{T}}$, $\hat{x}_6 = \hat{D}_{\Omega}$, $\bar{e}_1 = [e_1^{\mathrm{T}}, e_2^{\mathrm{T}}, e_5^{\mathrm{T}}]^{\mathrm{T}}$ is the estimation error vector and $\mathcal{E}_1 = [\bar{e}_1, 0_{9\times8}] \in \mathfrak{R}^{9\times9}$. $\mathcal{E}_2$ is the vector for the absolute values of each of the variables in the error $\bar{e}_1$, and υ_0 is the frational order. $\hat{\mathcal{X}}_1 = [x_2^{\mathrm{T}}, (R_b^e F/m + g\vartheta)^{\mathrm{T}}, (f_1 + g_1\hat{\varpi}_2)^{\mathrm{T}}]^{\mathrm{T}}$. $\bar{\beta}_1 \in \mathfrak{R}^{9\times9} > 0$, $\bar{\beta}_2 \in \mathfrak{R}^{9\times9} > 0$, $\bar{\beta}_3 \in \mathfrak{R}^{9\times9} > 0$ and $\bar{\beta}_4 \in \mathfrak{R}^{9\times9} > 0$ are the diagonal constant matrices.

Moreover, the errors are defined as $e_3 = \hat{x}_3 - x_3$, $e_4 = \hat{x}_4 - x_4$ and $e_6 = \hat{x}_6 - x_6$. Then the time derivatives of $\bar{e}_1$ and $\bar{e}_2 = [e_3^{\mathrm{T}}, e_4^{\mathrm{T}}, e_6^{\mathrm{T}}]^{\mathrm{T}}$ are given by

$$\begin{aligned} \dot{\bar{e}}_1 &= \bar{e}_2 + \tilde{\mathcal{X}}_1 - \bar{\beta}_1\mathcal{E}_1 I_f^{-\upsilon_0}\mathcal{E}_2 - \bar{\beta}_2\bar{e}_1 - \left\|g_1\right\|^2\bar{e}_1 \\ \dot{\bar{e}}_2 &= -\bar{\beta}_3\bar{e}_1 - h^*(t) - \bar{\beta}_4(\bar{e}_2 + \bar{x}_2) \end{aligned} \tag{19}$$

where the vector $\tilde{\mathcal{X}}_1 = \hat{\mathcal{X}}_1 - \mathcal{X}_1 = [0, \cdots, 0, (-g_1\tilde{\varpi}_2)^{\mathrm{T}}]^{\mathrm{T}} \in \mathfrak{R}^9$ and $\tilde{\varpi}_2 = \varpi_2 - \hat{\varpi}_2$. On the error system (19), the effectiveness of the fractional-order ESO is analyzed in the section on the system stability analysis.

Remark 3. The advantage of the fractional-order controller over the traditional controller is that fractional-order controller has more flexible regulation performance[40]. Therefore, the fractional-order term is introduced to increase the degree of freedom for the designed observers.

4 | TRAJECTORY TRACKING CONTROLLER DESIGN AND STABILITY ANALYSIS

In this section, on the basis of the PPM and ESO, the backstepping method is applied to develop the trajectory controller to track the desired three-dimensional trajectory planned by the trajectory planning algorithm. To facilitate the design of the TTC scheme, the UAH's model is divided into four subsystems, which are described in the following sections, and the corresponding controller of each subsystem is designed.

4.1 | Three-dimensional Trajectory Planning

According to the results of the WPA[41,42], an improved WPA is used to plan the desired trajectory from the start point to the destination point. Compared with the traditional WPA[43], the improved WPA has better faster convergence speed and the global optimization ability. The specific planning steps of the improved WPA is shown in Table 1 .

4.2 | Altitude Subsystem

According to the vertical dynamics in system (15), which is described as

$$\begin{aligned} \dot{z} &= w + d_z \\ \dot{w} &= g - \frac{1}{m}\cos\phi\cos\theta T_{mr} + d_w \end{aligned} \tag{20}$$

TABLE 1 Path planning by utilizing the improved WPA

Remark	The path of unmanned helicopter can be defined as the collection of a series of three-dimensional position point vector $\mathcal{P} = \{\mathcal{P}_s, \mathcal{P}_1, \mathcal{P}_2, ..., \mathcal{P}_g\}$, where $\mathcal{P}_s$ and $\mathcal{P}_g$ represent the start point and the destination point, respectively. $\mathcal{P}_i = (x_i, y_i, z_i), i = 1, 2, ...$ denotes the intermediate path point. Then take $\mathcal{P}_i$ as the position information of the wolf in three-dimensional space for the improved WPA method.
Step 1	**Parameters initialization**. Initialize the position of wolfs, the maximum iterations, update scale factor, population number, scale factor, distance determination, and maximum number of migration walks.
Step 2	The fitness value of objective function is calculated for the individual of the initial population, and one with the best value is chosen as the initial head wolf. The migration behavior is performed until the fitness value of a probe wolf is better than the current head wolf or reaches the maximum migration steps, and turn to **Step 3**.
Step 3	The wolves except the head wolf is randomly selected as the fierce wolves, and the fierce Wolf rushes to the prey position based on the summoning behavior location. On the way, if the value sensed by the fierce wolf is greater than the head wolf, the head wolf is replaced by the current fierce wolf to restart the summoning behavior; if the value is less than the head wolf, continue to rush until the distance between the fierce wolf and the head wolf is less than the critical distance, and turn to **Step 4**.
Step 4	The probe wolves and the fierce wolves jointly detect the position of the prey (i.e. the position of the head wolf), and the corresponding position is updated for the wolves participating in the siege.
Step 5	In the step, whether the number of iterations reaches the maximum number of iterations is further judged. If it is satisfied, the head wolf position is output, that is, the coordinates of the optimal path points, otherwise turn to **Step 2**.

According to (8), one can obtain

$$\dot{\beta}_z = \bar{\rho}_z \Pi_z (\dot{z}_d - w - d_z) - \dot{\bar{\rho}}_z \Pi_z e_z \tag{21}$$

Then, a detailed control scheme for the attitude subsystem (20) is proposed by utilizing the backstepping approach.

Step 1: The variables are defined as $z_z = \beta_z$ and $e_w = w_d - w$, where w_d denotes the virtual control law. Then, the time derivative of z_z can be written as

$$\dot{z}_z = \bar{\rho}_z \Pi_z (\dot{z}_d - w_d + e_w - d_z) - \dot{\bar{\rho}}_z \Pi_z e_z \tag{22}$$

From (22), the virtual control law w_d is constructed as

$$w_d = (\bar{\rho}_z \Pi_z)^{-1} [k_1 z_z + \bar{\rho}_z \Pi_z \dot{z}_d - \dot{\bar{\rho}}_z \Pi_z e_z - \bar{\rho}_z \Pi_z \hat{d}_z + z_z (\bar{\rho}_z \Pi_z)^2 \tanh((z_z \bar{\rho}_z \Pi_z)^2 / \mathcal{M}_z)] \tag{23}$$

where $k_1 > 0$ and $\mathcal{M}_z > 0$ are the designed parameters.

Substituting (24) into (22), one can obtain

$$\dot{z}_z = -k_1 z_z + \bar{\rho}_z \Pi_z \tilde{d}_z + \bar{\rho}_z \Pi_z e_w - z_z (\bar{\rho}_z \Pi_z)^2 \tanh((z_z \bar{\rho}_z \Pi_z)^2 / \mathcal{M}_z) \tag{24}$$

Step 2: Taking the time derivative of e_w, one has

$$\dot{e}_w = \dot{w}_d - g + \frac{1}{m} \cos\phi \cos\theta T_{mr} - d_w \tag{25}$$

To avoid the direct derivation of w_d in the design of the subsequent controller, the dynamic surface control method (DSCM) is employed to drive w_d through the first-order filter ζ_w in the following form:

$$t_w \dot{\zeta}_w + \zeta_w = w_d, \zeta_w(0) = w_d(0) \tag{26}$$

where $t_w > 0$ is the filter time constant.

Defining the filter error as $e_{\zeta_w} = \zeta_w - w_d$, and the derivative of e_{ζ_w} is written as $\dot{e}_{\zeta_w} = -t_w^{-1} e_{\zeta_w} + M_1(z_z, \dot{z}_d, e_z, \hat{d}_z, \bar{\rho}_z, \Pi_z)$, where $M_1(z_z, \dot{z}_d, e_z, \hat{d}_z, \bar{\rho}_z, \Pi_z)$ is the smooth function consisting of partial derivatives of the corresponding variables in a compact set. Then for a given initial condition, the function $M_1(z_z, \dot{z}_d, e_z, \hat{d}_z, \bar{\rho}_z, \Pi_z)$ is bounded in the compact set[44]. Hence, we have $|M_1(z_z, \dot{z}_d, e_z, \hat{d}_z, \bar{\rho}_z, \Pi_z)| \leq \bar{M}_1$, where $\bar{M}_1$ is a positive constant. Then, the corresponding control input T_{mr} based on the

fractional therory is designed as

$$T_{mr} = \frac{m}{\cos\phi\cos\theta}(-k_{21}e_w - \dot{\zeta}_w + g + \hat{d}_w - \rho_z\Pi_z z_z - k_{22}e_w I_f^{-\upsilon_z}|e_w|) \tag{27}$$

where $k_{21} > 0$ and $k_{22} > 0$ are the designed controller parameters, and υ_z is the fractional order.

Substituting (27) into (25), we can obtain that $\dot{e}_w = -k_{21}e_w + \tilde{d}_w - \bar{\rho}_z\Pi_z z_z + t_w^{-1}e_{\zeta_w} - k_{22}e_w I_f^{-\upsilon_z}|e_w| - M_1(z_z, \dot{z}_d, e_z, \hat{d}_z, \bar{\rho}_z, \Pi_z)$. Then, in order to facilitate the subsequent system stability analysis, the Lyapunov function for the altitude subsystem is selected as

$$V_1 = \frac{1}{2}z_z^2 + \frac{1}{2}e_w^2 + \frac{1}{2}e_{\zeta_w}^2 \tag{28}$$

Based on Lemma 2 and the analysis above, the time derivative of V_1 can satisfy that

$$\begin{aligned}\dot{V}_1 &= z_z\dot{z}_z + e_w\dot{e}_w + e_{\zeta_w}\dot{e}_{\zeta_w} \\ &\leq -(k_{21} - 1.5)e_w^2 - (t_w^{-1} - 0.5t_w^{-2} - 0.5)e_{\zeta_w}^2 - k_1 z_z^2 + 0.5\tilde{d}_z^2 + 0.5\tilde{d}_w^2 + 0.2758\mathcal{M}_z + \bar{M}_1^2\end{aligned} \tag{29}$$

where $(z_z\bar{\rho}_z\Pi_z)^2 - (z_z\bar{\rho}_z\Pi_z)^2\tanh((z_z\bar{\rho}_z\Pi_z)^2/\mathcal{M}_z \leq 0.2758\mathcal{M}_z$ based on the result in[45].

4.3 | Yaw Subsystem

Considering the yaw angle model in (15) as follows:

$$\dot{\psi} = H_3\varpi_1 = \frac{\sin\phi}{\cos\theta}q + \frac{\cos\phi}{\cos\theta}r \tag{30}$$

where H_3 represents the third row of matrix H.

According to (8), one has

$$\dot{\beta}_\psi = \bar{\rho}_\psi\Pi_\psi(\dot{\psi}_d - \frac{\sin\phi}{\cos\theta}q - \frac{\cos\phi}{\cos\theta}r) - \dot{\bar{\rho}}_\psi\Pi_\psi e_\psi \tag{31}$$

The variables are defined as $z_\psi = \beta_\psi$ and $e_r = r_d - r$, where r_d is desired yaw angle rate. The time derivative of z_ψ can be written as

$$\dot{z}_\psi = \bar{\rho}_\psi\Pi_\psi(\dot{\psi}_d - \frac{\sin\phi}{\cos\theta}q - \frac{\cos\phi}{\cos\theta}(r_d - e_r)) - \dot{\bar{\rho}}_\psi\Pi_\psi e_\psi \tag{32}$$

From (32), the desired yaw angle rate r_d is designed as

$$r_d = (\bar{\rho}_\psi\Pi_\psi\frac{\cos\phi}{\cos\theta})^{-1}[k_3 z_\psi - \bar{\rho}_\psi\Pi_\psi\frac{\sin\phi}{\cos\theta}q + \bar{\rho}_\psi\Pi_\psi\dot{\psi}_d - \dot{\bar{\rho}}_\psi\Pi_\psi e_\psi] \tag{33}$$

where $k_3 > 0$ is the designed parameters.

According to (32) and (33), one has that $\dot{z}_\psi = -k_3 z_\psi + k(\phi,\theta)e_\Omega$, where $k(\phi,\theta) = \left[0\ 0\ \rho_\psi\Pi_\psi\frac{\cos\phi}{\cos\theta}\right]$, $e_\Omega = [e_p, e_q, e_r]^{\mathrm{T}}$, $e_p = p_d - p$, $e_q = q_d - q$, p_d and q_d are the desired roll rate and pitch rate, respectively. Then, to facilitate the stability analysis for the subsequent system, the Lyapunov function for the altitude subsystem is chosen as

$$V_2 = \frac{1}{2}z_\psi^2 \tag{34}$$

Based on the analysis above, one has

$$\dot{V}_2 = -k_3 z_\psi^2 + z_\psi k(\phi,\theta)e_\Omega \tag{35}$$

4.4 | Horizontal Subsystem

The following horizontal model in (15) is written as:

$$\begin{aligned}\dot{\mathcal{P}}_1 &= \mathcal{V}_1 + D_{\mathcal{P}_1} \\ \dot{\mathcal{V}}_1 &= -\frac{1}{m}\gamma T_{mr} + D_{\mathcal{V}_1}\end{aligned} \tag{36}$$

where $\mathcal{P}_1 = [x, y]^{\mathrm{T}}$, $\mathcal{V}_1 = [u, v]^{\mathrm{T}}$, $D_{\mathcal{P}_1} = [d_x, d_y]^{\mathrm{T}}$, $D_{\mathcal{V}_1} = [d_u, d_v]^{\mathrm{T}}$, $\gamma = \begin{bmatrix} S_\phi S_\psi + C_\phi S_\theta C_\psi \\ -S_\phi C_\psi + C_\phi S_\theta S_\psi \end{bmatrix}$, $S_\bullet$ and $C_\bullet$ are the trigonometric functions for $\sin(\bullet)$ and $\cos(\bullet)$, respectively. To facilitate the study of the controller design, the direction model[46] is introduced as follows:

$$\dot{\gamma} = N\Omega_1 \tag{37}$$

where $\Omega_1 = [p, q]^{\mathrm{T}}$, $N = \begin{bmatrix} C_\phi S_\psi - S_\phi S_\theta C_\psi & C_\theta C_\psi \\ -C_\phi C_\psi - S_\phi S_\theta S_\psi & C_\theta S_\psi \end{bmatrix}$.

According to (8), we have

$$\dot{\beta}_{1,2} = \bar{\rho}_{1,2}\Pi_{1,2}(\dot{\mathcal{P}}_{1d} - \mathcal{V}_1 - D_{\mathcal{P}_1}) - \dot{\bar{\rho}}_{1,2}\Pi_{1,2}e_{1,2} \tag{38}$$

where $\beta_{1,2} = [\beta_x, \beta_y]^{\mathrm{T}}$, $\Pi_{1,2} = \mathrm{diag}\{\Pi_x, \Pi_y\}$, $\bar{\rho}_{1,2} = \mathrm{diag}\{\bar{\rho}_x, \bar{\rho}_y\}$, and $\dot{P}_{1d} = [x_d, y_d]^{\mathrm{T}}$.

The variables are defined as $z_{\mathcal{P}_1} = \beta_{1,2}$ and $e_{\mathcal{V}_1} = \mathcal{V}_{1d} - \mathcal{V}_1$, where $\mathcal{V}_{1d}$ is the desired forward and lateral translation speed, $\beta_{1,2}$ is the transformed error vector. Then, a detailed control scheme for the attitude subsystem (38) is designed by utilizing the backstepping approach.

Step 1: Taking the time derivative of $z_{\mathcal{P}_1}$, we can obtain

$$\dot{z}_{\mathcal{P}_1} = \bar{\rho}_{1,2}\Pi_{1,2}(\dot{\mathcal{P}}_{1d} - \mathcal{V}_{1d} + e_{\mathcal{V}1} - D_{\mathcal{P}_1}) - \dot{\bar{\rho}}_{1,2}\Pi_{1,2}e_{\mathcal{P}_1} \tag{39}$$

From (39), the virtual control law $\mathcal{V}_{1d}$ is designed as

$$\begin{aligned} \mathcal{V}_{1d} = {} & (\bar{\rho}_{1,2}\Pi_{1,2})^{-1}[K_4 z_{\mathcal{P}_1} + \bar{\rho}_{1,2}\Pi_{1,2}(\dot{\mathcal{P}}_{1d} - \hat{D}_{\mathcal{P}1}) \\ & + z_{\mathcal{P}_1}\left\|\bar{\rho}_{1,2}\Pi_{1,2}\right\|^2 \tanh\left(\left\|\bar{\rho}_{1,2}\Pi_{1,2}z_{\mathcal{P}_1}\right\|^2/\mathcal{M}_{\mathcal{P}}\right) - \dot{\bar{\rho}}_{1,2}\Pi_{1,2}e_{\mathcal{P}_1}] \end{aligned} \tag{40}$$

where $K_4 \in \mathfrak{R}^{2\times 2}$ is the designed gain diagonal matrix, $\mathcal{M}_{\mathcal{P}}$ is a positive constant, and $\hat{D}_{\mathcal{P}1} = [\hat{d}_x, \hat{d}_y]^{\mathrm{T}}$. The variable $\tilde{D}_{\mathcal{P}_1}$ is defined as $\tilde{D}_{\mathcal{P}_1} = [\tilde{d}_x, \tilde{d}_y]^{\mathrm{T}}$.

Substituting (40) into (39), one has

$$\dot{z}_{\mathcal{P}_1} = -z_{\mathcal{P}_1}\left\|\bar{\rho}_{1,2}\Pi_{1,2}\right\|^2 \tanh\left(\left\|\bar{\rho}_{1,2}\Pi_{1,2}z_{\mathcal{P}_1}\right\|^2/\mathcal{M}_{\mathcal{P}}\right) - K_4 z_{\mathcal{P}_1} + \bar{\rho}_{1,2}\Pi_{1,2}\tilde{D}_{\mathcal{P}_1} + \bar{\rho}_{1,2}\Pi_{1,2}e_{\mathcal{V}_1} \tag{41}$$

Step 2: Taking the time derivative of $e_{\mathcal{V}_1}$, it yields

$$\dot{e}_{\mathcal{V}_1} = \dot{\mathcal{V}}_{1d} - \dot{\mathcal{V}}_1 = \dot{\mathcal{V}}_{1d} + \frac{1}{m}\gamma T_{mr} - D_{\mathcal{V}_1} \tag{42}$$

Defining the direction tracking error as $e_\gamma = \gamma_d - \gamma$, where γ_d is the desired direction pointing vector. Then we can obtain that $\dot{e}_{\mathcal{V}_1} = \dot{\mathcal{V}}_{1d} + \frac{1}{m}\gamma_d T_{mr} - \frac{1}{m}e_\gamma T_{mr} - D_{\mathcal{V}_1}$. To avoid the direct derivation of V_{1d} in the design of the subsequent controller, the DSCM is employed to drive $\mathcal{V}_{1d}$ through the first-order filter $\zeta_{\mathcal{V}_1}$ in the following form:

$$t_{\mathcal{V}_1}\dot{\zeta}_{\mathcal{V}_1} + \zeta_{\mathcal{V}_1} = \mathcal{V}_{1d}, \zeta_{\mathcal{V}_1}(0) = \mathcal{V}_{1d}(0) \tag{43}$$

where $t_{\mathcal{V}_1} > 0$ is the filter time diagonal matrix.

Defining the filter error as $e_{\zeta_{\mathcal{V}_1}} = \zeta_{\mathcal{V}_1} - \mathcal{V}_{1d}$, and the derivative of $e_{\zeta_{\mathcal{V}_1}}$ is written as $\dot{e}_{\zeta_{\mathcal{V}_1}} = -t_{\mathcal{V}_1}^{-1}e_{\zeta_{\mathcal{V}_1}} + M_2(z_{\mathcal{P}_1}, \dot{\mathcal{P}}_{1d}, e_{\mathcal{P}_1}, \hat{D}_{\mathcal{P}_1}, \bar{\rho}_{1,2}, \Pi_{1,2})$, where $M_2(z_{\mathcal{P}_1}, \dot{\mathcal{P}}_{1d}, e_{\mathcal{P}_1}, \hat{D}_{\mathcal{P}_1}, \bar{\rho}_{1,2}, \Pi_{1,2})$ is the smooth function vector consisting of partial derivatives of the corresponding variables in a compact set[44]. Then for a given initial condition, the function $M_2(z_{\mathcal{P}_1}, \dot{\mathcal{P}}_{1d}, e_{\mathcal{P}_1}, \hat{D}_{\mathcal{P}_1}, \bar{\rho}_{1,2}, \Pi_{1,2})$ is bounded in the compact set[44]. Hence, we have $\|M_2(z_{\mathcal{P}_1}, \dot{\mathcal{P}}_{1d}, e_{\mathcal{P}_1}, \hat{D}_{\mathcal{P}_1}, \bar{\rho}_{1,2}, \Pi_{1,2})\| \le \bar{M}_2$, where $\bar{M}_2$ is a positive constant. Then, the corresponding virtual control law γ_d is designed as

$$\gamma_d = \frac{m}{T_{mr}}(-K_5 e_{\mathcal{V}_1} - \dot{\zeta}_{\mathcal{V}_1} + \hat{D}_{\mathcal{V}_1} - \bar{\rho}_{1,2}\Pi_{1,2}z_{\mathcal{P}_1}) \tag{44}$$

where $K_5 \in \mathfrak{R}^{2\times 2}$ is the designed diagonal matrix, and $\hat{D}_{\mathcal{V}1} = [\hat{d}_u, \hat{d}_v]^{\mathrm{T}}$. The variable $\tilde{D}_{\mathcal{V}_1}$ is defined as $\tilde{D}_{\mathcal{V}_1} = [\tilde{d}_u, \tilde{d}_v]^{\mathrm{T}}$.

Substituting (44) into (42), we can obtain

$$\dot{e}_{\mathcal{V}_1} = -K_5 e_{\mathcal{V}_1} + \tilde{D}_{\mathcal{V}_1} - \frac{1}{m}e_\gamma T_{mr} - \bar{\rho}_{1,2}\Pi_{1,2}z_{\mathcal{P}_1} + t_{\mathcal{V}_1}^{-1}e_{\zeta_{\mathcal{V}_1}} - M_2(z_{\mathcal{P}_1}, \dot{\mathcal{P}}_{1d}, e_{\mathcal{P}_1}, \hat{D}_{\mathcal{P}_1}, \bar{\rho}_{1,2}, \Pi_{1,2}) \tag{45}$$

Step 3: According to (37), the derivative of e_γ is written as $\dot{e}_\gamma = \dot{\gamma}_d - \dot{\gamma} = \dot{\gamma}_d - N\Omega_1$. Then the error is defined as $e_{\Omega_1} = \Omega_{1d} - \Omega_1$, where $\Omega_{1d} = [p_d, q_d]^{\mathrm{T}}$ will be designed in the following analysis. Furthermore, one has that

$$\dot{e}_\gamma = \dot{\gamma}_d - N\Omega_{1d} + N_0 e_\Omega \tag{46}$$

where the variable $N_0 = \begin{bmatrix} N & 0_{2\times 1} \end{bmatrix}$. To avoid the direct derivation of γ_d in the design of the subsequent controller, the DSCM is employed to drive γ_d through the first-order filter ζ_γ in the following form:

$$t_\gamma\dot{\zeta}_\gamma + \zeta_\gamma = \gamma_d, \zeta_\gamma(0) = \gamma_d(0) \tag{47}$$

where $t_\gamma > 0$ is the filter time diagonal matrix.

Defining the filter error as $e_{\zeta_\gamma} = \zeta_\gamma - \gamma_d$ and the derivative of e_{ζ_γ} is written as $\dot{e}_{\zeta_\gamma} = -t_\gamma^{-1} e_{\zeta_\gamma} + M_3(e_{\nu_1}, \dot{\zeta}_{\nu_1}, z_{\mathcal{P}_1}, \hat{D}_{\nu_1}, \bar{\rho}_{1,2}, \Pi_{1,2})$, where $M_3(e_{\nu_1}, \dot{\zeta}_{\nu_1}, z_{\mathcal{P}_1}, \hat{D}_{\nu_1}, \bar{\rho}_{1,2}, \Pi_{1,2})$ is the smooth function vector consisting of partial derivatives of the corresponding variables in a compact set. Then for a given initial condition, the function $M_3(e_{\nu_1}, \dot{\zeta}_{\nu_1}, z_{\mathcal{P}_1}, \hat{D}_{\nu_1}, \bar{\rho}_{1,2}, \Pi_{1,2})$ is bounded in the compact set. Hence, we have that $\|M_3(e_{\nu_1}, \dot{\zeta}_{\nu_1}, z_{\mathcal{P}_1}, \hat{D}_{\nu_1}, \bar{\rho}_{1,2}, \Pi_{1,2})\| \leq \bar{M}_3$, where $\bar{M}_3$ is a positive constant. Then the vector Ω_{1d} is designed as

$$\Omega_{1d} = N^{-1}(K_6 e_\gamma + \dot{\zeta}_\gamma - \frac{1}{m} T_{mr} e_{V_1}) \tag{48}$$

where $K_6 \in \mathfrak{R}^{2\times 2}$ is the designed diagonal matrix.

From (46) and (48), one has

$$\dot{e}_\gamma = -K_6 e_\gamma + N_0 e_\Omega + \frac{1}{m} T_{mr} e_{\nu_1} + t_\gamma^{-1} e_{\zeta_\gamma} - M_3(e_{\nu_1}, \dot{\zeta}_{\nu_1}, z_{\mathcal{P}_1}, \hat{D}_{\nu_1}, \bar{\rho}_{1,2}, \Pi_{1,2}) \tag{49}$$

Then, to facilitate the stability analysis of the subsequent system, the Lyapunov function for the horizontal subsystem is chosen as $V_3 = \frac{1}{2} z_{\mathcal{P}_1}^{\mathrm{T}} z_{\mathcal{P}_1} + \frac{1}{2} e_{\nu_1}^{\mathrm{T}} e_{\nu_1} + \frac{1}{2} e_\gamma^{\mathrm{T}} e_\gamma + \frac{1}{2} e_{\zeta_{\nu_1}}^{\mathrm{T}} e_{\zeta_{\nu_1}} + \frac{1}{2} e_{\zeta_\gamma}^{\mathrm{T}} e_{\zeta_\gamma}$. Then, based on the analysis above, the time derivative of the V_3 can be written as

$$\begin{aligned}
\dot{V}_3 &= z_{\mathcal{P}_1}^{\mathrm{T}} \dot{z}_{\mathcal{P}_1} + e_{\nu_1}^{\mathrm{T}} \dot{e}_{\nu_1} + e_\gamma^{\mathrm{T}} \dot{e}_\gamma + e_{\zeta_{\nu_1}}^{\mathrm{T}} \dot{e}_{\zeta_{\nu_1}} + e_{\zeta_\gamma}^{\mathrm{T}} \dot{e}_{\zeta_\gamma} \\
&\leq -\lambda_{\min}(K_4) \left\| z_{\mathcal{P}_1} \right\|^2 - (\lambda_{\min}(K_5) - 1.5) \left\| e_{\nu_1} \right\|^2 - (\lambda_{\min}(K_6) - 1) \left\| e_\gamma \right\|^2 - (\lambda_{\min}(t_{\nu_1}^{-1}) - 0.5 \\
&\quad - 0.5(\lambda_{\max}(t_{\nu_1}^{-1}))^2) \left\| e_{\zeta_{\nu_1}} \right\|^2 + 0.5 \left\| \tilde{D}_{\mathcal{P}_1} \right\|^2 + \bar{M}_3^2 - (\lambda_{\min}(t_\gamma^{-1}) - 0.5(\lambda_{\max}(t_\gamma^{-1}))^2 - 0.5) \left\| e_{\zeta_\gamma} \right\|^2 \\
&\quad + e_\gamma^{\mathrm{T}} N_0 e_\Omega + 0.2758 M_{\mathcal{P}} + \bar{M}_2^2 + 0.5 \left\| \tilde{D}_{\nu_1} \right\|^2
\end{aligned} \tag{50}$$

where $\lambda_{\max}(\bullet)$ and $\lambda_{\min}(\bullet)$ denote the largest and smallest eigenvalues of the matrices, respectively.

4.5 | Attitude Angular Rate And Rotor Flapping Dynamics Subsystem

Considering the relevant model in (15) as follows:

$$\begin{aligned}
\dot{\varpi}_1 &= f_1 + g_1 \varpi_2 + D_\Omega \\
\dot{\varpi}_2 &= \Gamma \varpi_2 + I \varpi_1 + g_2 u_f
\end{aligned} \tag{51}$$

The variables are defined as $e_\Omega = \varpi_{1d} - \varpi_1$ and $e_u = \varpi_{2d} - \hat{\varpi}_2$, where $\varpi_{1d} = [p_d, q_d, r_d]^{\mathrm{T}}$ is the desired signal vector and its value can be obtained from subsection B and C. ϖ_{2d} is the virtual control law. Then, a detailed control scheme for the attitude subsystem (51) is designed by utilizing the backstepping approach.

Step 1: Taking the time derivative of e_Ω, we can obtain

$$\dot{e}_\Omega = \dot{\varpi}_{1d} - f_1 - g_1 \varpi_{2d} + g_1 e_u - D_\Omega - g_1 \tilde{\varpi}_2 \tag{52}$$

To avoid the direct derivation of ϖ_{1d} in the subsequent controller design, the DSCM is employed to drive ϖ_{1d} through the first-order filter ζ_{ϖ_1} in the following form:

$$t_{\varpi_1} \dot{\zeta}_{\varpi_1} + \zeta_{\varpi_1} = \varpi_{1d}, \zeta_{\varpi_1}(0) = \varpi_{1d}(0) \tag{53}$$

where $t_{\varpi_1} > 0$ is the filter time diagonal matrix.

Defining the filter error as $e_{\zeta_{\varpi_1}} = \zeta_{\varpi_1} - \varpi_{1d}$, and taking the time derivative of $e_{\zeta_{\varpi_1}}$, one has that $\dot{e}_{\zeta_{\varpi_1}} = -t_{\varpi_1}^{-1} e_{\zeta_{\varpi_1}} + M_4(z_\psi, \dot{\psi}_d, e_\psi, e_\gamma, \dot{\zeta}_\gamma, e_{\nu_1}, \bar{\rho}_\psi, \Pi_\psi)$, where $M_4(z_\psi, \dot{\psi}_d, e_\psi, e_\gamma, \dot{\zeta}_\gamma, e_{\nu_1}, \bar{\rho}_\psi, \Pi_\psi)$ is the smooth function vector consisting of partial derivatives of the corresponding variables in a compact set. Then for a given initial condition, the function $M_4(z_\psi, \dot{\psi}_d, e_\psi, e_\gamma, \dot{\zeta}_\gamma, e_{\nu_1}, \bar{\rho}_\psi, \Pi_\psi)$ is bounded in the compact set[44]. Hence, we have $\|M_4(z_\psi, \dot{\psi}_d, e_\psi, e_\gamma, \dot{\zeta}_\gamma, e_{\nu_1}, \bar{\rho}_\psi, \Pi_\psi)\| \leq \bar{M}_4$, where $\bar{M}_4$ is a positive constant. Then, the corresponding virtual control law ϖ_{2d} is designed as

$$\varpi_{2d} = g_1^{-1}(K_7 e_\Omega + \dot{\zeta}_{\varpi_1} - f_1 - \hat{D}_\Omega + k^{\mathrm{T}}(\phi, \theta) z_\psi + N_0^{\mathrm{T}} e_\gamma + \left\| g_1 \right\|^2 e_\Omega) \tag{54}$$

where $K_7 \in \mathfrak{R}^{3\times 3}$ is the diagonal matrix.

Substituting (54) into (51), one can obtain

$$\dot{e}_\Omega = -K_7 e_\Omega + \tilde{D}_\Omega + g_1 e_u - k^{\mathrm{T}}(\phi, \theta) z_\psi - N_0^{\mathrm{T}} e_\gamma - M_4(z_\psi, \dot{\psi}_d, e_\psi, e_\gamma, \dot{\zeta}_\gamma, e_{\nu_1}, \bar{\rho}_\psi, \Pi_\psi) + t_{\varpi_1}^{-1} e_{\zeta_{\varpi_1}} - g_1 \tilde{\varpi}_2 - \left\| g_1 \right\|^2 e_\Omega \tag{55}$$

Step 2: Taking the time derivative of e_u, it yields

$$\dot{e}_u = \dot{\varpi}_{2d} - \Gamma\varpi_2 - I\varpi_1 - g_2 u_f \tag{56}$$

To avoid the direct derivation of ϖ_{2d} in the design of the subsequent controller, the DSCM is employed to drive ϖ_{2d} through the first-order filter ζ_{ϖ_2} in the following form:

$$t_{\varpi_2}\dot{\zeta}_{\varpi_2} + \zeta_{\varpi_2} = \varpi_{2d}, \zeta_{\varpi_2}(0) = \varpi_{2d}(0) \tag{57}$$

where $t_{\varpi_2} > 0$ is the filter time diagonal matrix.

Defining the filter error as $e_{\zeta_{\varpi_2}} = \zeta_{\varpi_2} - \varpi_{2d}$, and the derivative of $e_{\zeta_{\varpi_2}}$ can be written as $\dot{e}_{\zeta_{\varpi_2}} = -t_{\varpi_2}^{-1} e_{\zeta_{\varpi_2}} + M_5(e_\Omega, \dot{\zeta}_{\varpi_1}, \hat{D}_\Omega, z_\psi, e_\gamma)$, where $M_5(e_\Omega, \dot{\zeta}_{\varpi_1}, \hat{D}_\Omega, z_\psi, e_\gamma)$ is the smooth function vector consisting of partial derivatives of the corresponding variables in a compact set. Then for a given initial condition, the function $M_5(e_\Omega, \dot{\zeta}_{\varpi_1}, \hat{D}_\Omega, z_\psi, e_\gamma)$ is bounded in the compact set[44]. Hence, we have $\|M_5(e_\Omega, \dot{\zeta}_{\varpi_1}, \hat{D}_\Omega, z_\psi, e_\gamma)\| \le \bar{M}_5$, where $\bar{M}_5$ is a positive constant. Then, the equivalent fatcional-order control input u_f can be designed as

$$u_f = g_2^{-1}[K_{81}e_u + \dot{\zeta}_{\varpi_2} - \Gamma\hat{\varpi}_2 - I\hat{\varpi}_1 + g_1^{\mathrm{T}} e_\Omega - \alpha_2(\varpi_1 - \hat{\varpi}_1) - K_{82}\bar{e}_u I_f^{-\upsilon_f}\mathcal{E}_u] \tag{58}$$

where $K_{81} \in \mathfrak{R}^{3\times3}$ and $K_{82} \in \mathfrak{R}^{3\times3}$ are the designed gain diagonal matrices, $\bar{e}_u = [e_u^{\mathrm{T}}, 0_{3\times2}] \in \mathfrak{R}^{3\times3}$, $\mathcal{E}_u$ is the vector for the absolute values of each of the variables in the error e_u, and υ_f is the frational order.

Substituting (58) into (56), one can obtain

$$\dot{e}_u = -K_{81}e_u - g_1^{\mathrm{T}} e_\Omega + t_{\varpi_2}^{-1} e_{\zeta_{\varpi_2}} - K_{82}\bar{e}_u I_f^{-\upsilon_f} E_u - M_5(e_\Omega, \dot{\zeta}_{\varpi_1}, \hat{D}_\Omega, z_\psi, e_\gamma) \tag{59}$$

Then, to facilitate the stability analysis of the subsequent system, the Lyapunov function for the horizontal subsystem is chosen as $V_4 = \frac{1}{2}e_\Omega^{\mathrm{T}} e_\Omega + \frac{1}{2}e_u^{\mathrm{T}} e_u + \frac{1}{2}e_{\zeta_{\varpi_1}}^{\mathrm{T}} e_{\zeta_{\varpi_1}} + \frac{1}{2}e_{\zeta_{\varpi_2}}^{\mathrm{T}} e_{\zeta_{\varpi_2}}$. Then, based on Lemma 2 and the analysis above, one can obtain that

$$\begin{aligned}\dot{V}_4 \le & -(\lambda_{\min}(K_7) - 1.5)\|e_\Omega\|^2 + 0.5\|\tilde{\varpi}_2\|^2 + \bar{M}_4^2 - (\lambda_{\min}(t_{\varpi_1}^{-1}) - 0.5(\lambda_{\min}(t_{\varpi_1}^{-1}))^2 - 0.5)\left\|e_{\zeta_{\varpi_1}}\right\|^2 \\ & - (\lambda_{\min}(t_{\varpi_2}^{-1}) - 0.5(\lambda_{\min}(t_{\varpi_2}^{-1}))^2 - 0.5)\left\|e_{\zeta_{\varpi_2}}\right\|^2 - e_\Omega^{\mathrm{T}} k^{\mathrm{T}}(\phi,\theta) z_\psi - e_\Omega^{\mathrm{T}} N_0^{\mathrm{T}} e_\gamma + 0.5\|\tilde{D}_\Omega\|^2 \\ & + \bar{M}_5^2 - (\lambda_{\min}(K_8) - 1)\|e_u\|^2\end{aligned} \tag{60}$$

4.6 | Stability Analysis

The above TTC design of the UAH with the unmeasurable states based on the PPM and the ESO can be summarized as the following theorem:

Theorem 1. Consider the nonlinear model of the UAH with the prescribed performance, the external bounded WGDs and the unmeasurable states espressed by (2). The fractional-order ESO is designed in the form of (18). The frational-order high-gain observer is designed as (13). By properly selecting the controller paremeters, the designed control signals (24), (27), (33), (40), (44), (48), (54) and (58) based on the PPM and the ESO can ultimately make the error signals of the entire system for the UAH uniformly bounded, and realize the tracking of the given periodic desired signal.

Proof: For the close-loop control system of the UAH, the Lyapunov function is choosen as

$$V = \frac{1}{2}\tilde{\varpi}_1^{\mathrm{T}}\tilde{\varpi}_1 + \frac{1}{2}\tilde{\varpi}_2^{\mathrm{T}}\tilde{\varpi}_2 + \frac{1}{2}\bar{e}_1^{\mathrm{T}}\bar{e}_1 + \frac{1}{2}\bar{e}_2^{\mathrm{T}}\bar{e}_2 + V_1 + V_2 + V_3 + V_4 \tag{61}$$

According to the analysis above, we can obtain

$$\begin{aligned}\dot{V} = & -\mathcal{K}_1\|\tilde{\varpi}_1\|^2 + \mathcal{K}_2\|\tilde{\varpi}_2\|^2 - \mathcal{K}_3\|\bar{e}_1\|^2 - \mathcal{K}_4\|\bar{e}_2\|^2 - \mathcal{K}_5 e_w^2 - \mathcal{K}_6 e_{\zeta_w}^2 - \mathcal{K}_7\left\|z_{P_1}\right\|^2 - \mathcal{K}_8\left\|e_{V_1}\right\|^2 \\ & - \mathcal{K}_9\left\|e_\gamma\right\|^2 - \mathcal{K}_{10}\left\|e_{\zeta_{V_1}}\right\|^2 - \mathcal{K}_{11}\left\|e_{\zeta_\gamma}\right\|^2 - \mathcal{K}_{12}\|e_\Omega\|^2 - \mathcal{K}_{13}\|e_u\|^2 - \mathcal{K}_{14}\left\|e_{\zeta_{\varpi_1}}\right\|^2 \\ & - \mathcal{K}_{15}\left\|e_{\zeta_{\varpi_2}}\right\|^2 - \mathcal{K}_{16} z_z^2 - \mathcal{K}_{17} z_\psi^2 - \mathcal{K}_{18}\end{aligned} \tag{62}$$

where $\mathcal{K}_1 = \lambda_{\min}(\alpha_1) - 0.5 - 0.5(\lambda_{\max}(\alpha_2))^2$, $\mathcal{K}_2 = \lambda_{\max}(\Gamma) + 2$, $\mathcal{K}_3 = \lambda_{\min}(\bar{\beta}_2) - 0.5 - 0.5(\lambda_{\max}(\bar{\beta}_3))^2$, $\mathcal{K}_4 = (\lambda_{\min}(\bar{\beta}_4) - 5.5)$, $\mathcal{K}_5 = k_{21} - 1.5$, $\mathcal{K}_6 = t_w^{-1} - 0.5t_w^{-2} - 0.5$, $\mathcal{K}_7 = \lambda_{\min}(K_4)$, $\mathcal{K}_8 = \lambda_{\min}(K_5) - 1.5$, $\mathcal{K}_9 = \lambda_{\min}(K_6) - 1$, $\mathcal{K}_{10} = \lambda_{\min}(t_{\gamma_1}^{-1}) - 0.5(\lambda_{\max}(t_{\gamma_1}^{-1}))^2 - 0.5$, $\mathcal{K}_{11} = \lambda_{\min}(t_\gamma^{-1}) - 0.5(\lambda_{\max}(t_\gamma^{-1}))^2 - 0.5$, $\mathcal{K}_{12} = \lambda_{\min}(K_7) - 1.5$, $\mathcal{K}_{13} = \lambda_{\min}(K_{81}) - 1$, $\mathcal{K}_{14} = \lambda_{\min}(t_{\varpi_1}^{-1}) - 0.5(\lambda_{\min}(t_{\varpi_1}^{-1}))^2 - 0.5$, $\mathcal{K}_{15} = \lambda_{\min}(t_{\varpi_2}^{-1}) - 0.5(\lambda_{\min}(t_{\varpi_2}^{-1}))^2 - 0.5$, $\mathcal{K}_{16} = k_1$, $\mathcal{K}_{17} = k_3$ and $\mathcal{K}_{18} = 0.2758M_z + 0.2758M_P + \bar{M}_1^2 + \bar{M}_2^2 + \bar{M}_3^2 + \bar{M}_4^2 +$

$\bar{M}_5^2 + 0.5\bar{h}_1^* + 0.5(\lambda_{\max}(\beta_4))^2\bar{h}_2^*$. On the basis of Assumption 2, we have that $\|h^*(t)\|^2 \leq \bar{h}_1^*$ and $\|\bar{x}_2\|^2 \leq \bar{h}_2^*$, where $\bar{h}_1^*$ and $\bar{h}_2^*$ are positive constants.

According to (62) and Lemma 1, when the parameters are reasonable, the error signals in the entire system are ultimately uniformly bounded.

5 | SIMULATION STUDY

In this section, some simulation studies are presented to illustrate the effectiveness of the developed TTC for the nonlinear model of the UAH. The simulations include two parts. In the first part, the three-dimensional trajectory of the UAH is planned by using the WPA algorithm to generate a three-dimensional space trajectory, and the corresponding comparison results of the different methods are given. In the second part, the trajectory in three-dimensional space is deemed as the desired signal, we explore whether the trajectory tracking controller based on the PPM and fractional-order ESO can effectively ensure that the three-dimensional space trajectory can be tracked, and the simulation comparisons are also presented.

5.1 | Three-dimensional Trajectory And Comparative Analysis

On the basis of the improved WPA described in Table 1 , the three-dimensional space trajectory is planned, and the result of the final planning trajectory is shown in Fig. 3 . In order to illustrate the superiority of using the improved WPA to plan three-dimensional trajectory in this paper, the traditional WPA, the traditional particle swarm optimization (PSO) algorithm and the genetic algorithm (GA)[47,48] are introduced for the three-dimensional trajectory planning, and the simulation results are shown in Figs. 4 -6 . According to the planned three-dimensional trajectory in Fig. 4 and Fig. 5 and the change curves of fitness values in Fig. 6 , we can be seen that the improved WPA has the better planned track quality, the shorter distance and the faster convergence speed than the traditional WPA, PSO and GA. Therefore, in the following simulation of the trajectory tracking, the trajectory planned by using the improved WPA is regarded as the desired tracking trajectory.

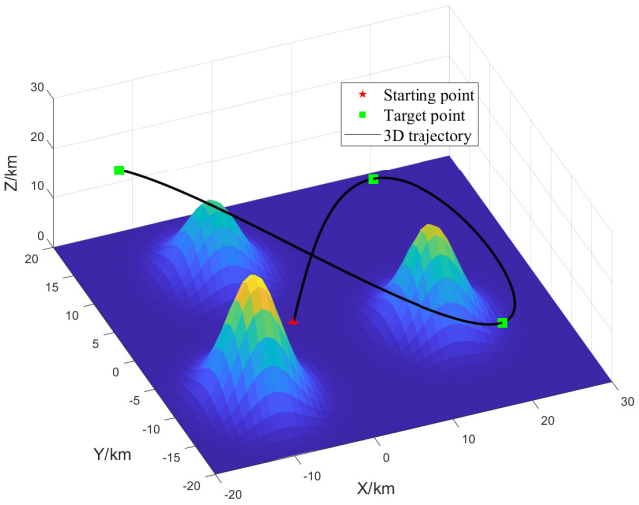

FIGURE 3 Three-dimensional space trajectory.

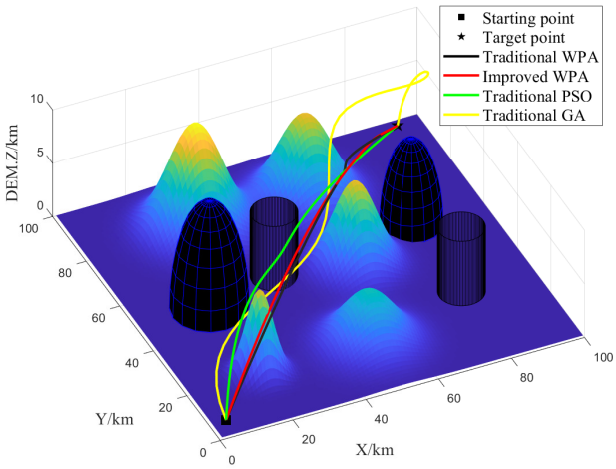

FIGURE 4 Front view of trajectory comparision.

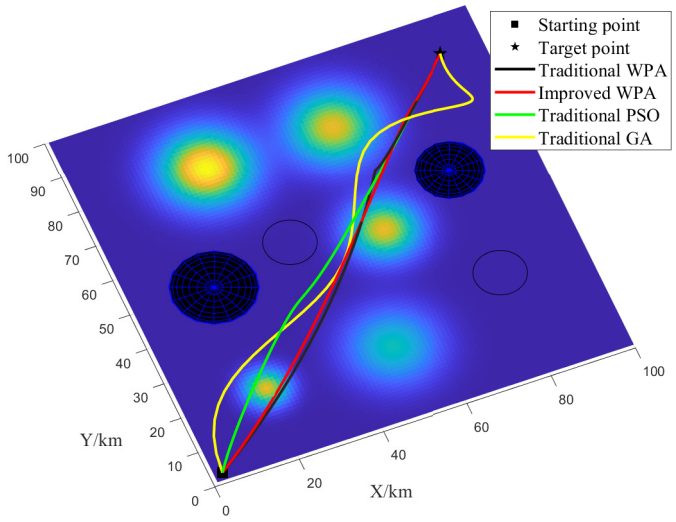

FIGURE 5 Top view of trajectory comparision.

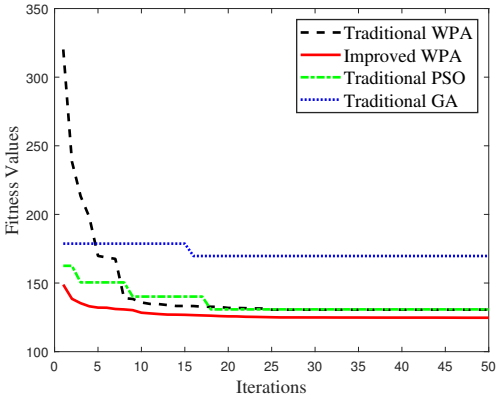

FIGURE 6 Curve of fitness value contrast change.

TABLE 2 Parameters of small-scale unmanned helicopter

Symbol	Unit	Value
m	kg	1.5
g	$\mathrm{m/s^2}$	9.8
(J_{xx}, J_{yy}, J_{zz})	$\mathrm{kg \cdot m^2}$	(0.025, 0.051, 0.04)
(L_x, L_y, L_z)	m	(0, 0, 0.09)
(H_x, H_z)	m	(0.03, 0.5)
(A_{lon}, B_{lat})	rad/ms	(2, 2)
C_m	$\mathrm{N \cdot m}$	32
C_k	$\mathrm{m/\sqrt{N}}$	0.01
D_k	$\mathrm{N \cdot m}$	0.4
τ_e	s	0.1

5.2 | Control Simulation and Comparation

To verify the effectiveness of the TTC scheme for the three-dimensional space trajectory, the UAH is deemed as the study object, and the basic parameters are given in Table 2 . The relevant parameters of the external wind gusts are choose as $V_{\mathcal{P}im} = 2\mathrm{m/s}$, $d_{\mathcal{P}i} = 100\mathrm{m}$, $i = x, y, z$. Specifically, the wind gust model of $D_{\mathcal{P}}$, $D_{\mathcal{V}}$ and D_{Ω} can be described as $D_{\mathcal{P}} = [1-\cos(0.03X), 1-\cos(0.03Y), 1-\cos(0.03Z)]^{\mathrm{T}}$, $D_{\mathcal{V}} = [0.03u\sin(0.03X), 0.03v\sin(0.03Y), 0.03w\sin(0.03Z)]^{\mathrm{T}}$, and $D_{\Omega} = [2\sin(0.2t), 3\sin(0.3t), 2\sin(0.1t)]^{\mathrm{T}}$. Besides, as the form shown in (4), the precribed performance function $\bar{\rho}_i$ is choosen as $\bar{\rho}_i = 2\exp(-t) + 0.1, i = 1, 2, 3, 4$, and the relevant designed parameters are selected as $\lambda_{1i} = \lambda_{2i} = 0.2$.

Futhermore, at the initial moment, the UAH hovers at point $(0, 0, 0)$ and the desired position input signal is given by the conclusion in the previous analysis. Meanwhile, the desired yaw angle input is selected as $\psi_d = 0$. The corresponding parameters of the fractional-order ESOs are choosen as $\bar{\beta}_1 = \bar{\beta}_2 = \mathrm{diag}\{60, 60, \cdots, 60\} \in \mathfrak{R}^{9\times9}$ and $\bar{\beta}_3 = \bar{\beta}_4 = \mathrm{diag}\{900, 900, \cdots, 900\} \in \mathfrak{R}^{9\times9}$. The relevant parameters of fractional-order observer are set as $A_i = 44$, $\tau_2 = 0.1$, $\alpha_0 = \alpha_1 = \mathrm{diag}\{1, 1, 1\} \in \mathfrak{R}^{3\times3}$, $\alpha_2 = \mathrm{diag}\{0.1, 0.1, 0.1\} \in \mathfrak{R}^{3\times3}$. The relevant parameters of the trajectory tracking controller are choosen as $k_1 = 4$, $k_{21} = k_{22} = 16$, $k_3 = 32$, $K_4 = \mathrm{diag}\{4, 4\}$, $K_5 = \mathrm{diag}\{16, 16\}$, $K_6 = \mathrm{diag}\{32, 32\}$, $K_7 = \mathrm{diag}\{50, 50, 50\}$, $K_{81} = K_{82} = \mathrm{diag}\{50, 50, 50\}$.

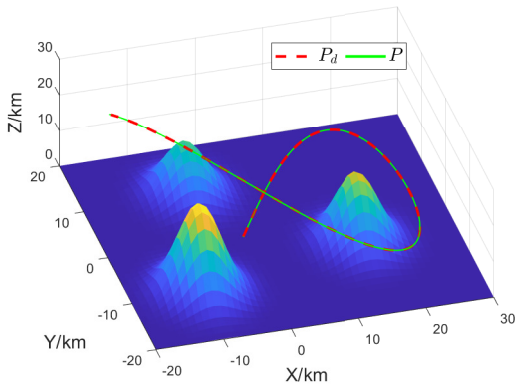

FIGURE 7 Tracking curves of position P.

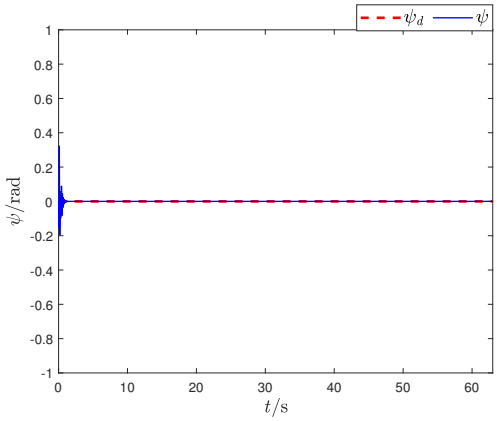

FIGURE 8 Tracking curves of yaw angle ψ.

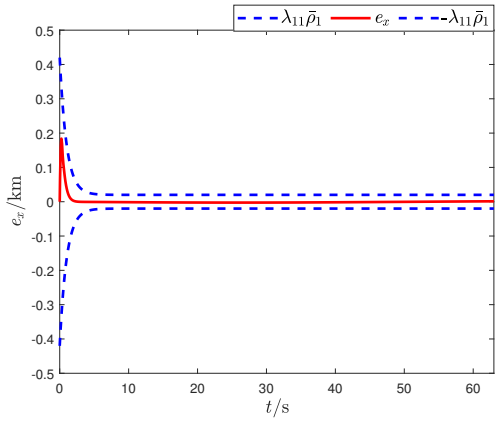

FIGURE 9 Error of e_x with precribed performance.

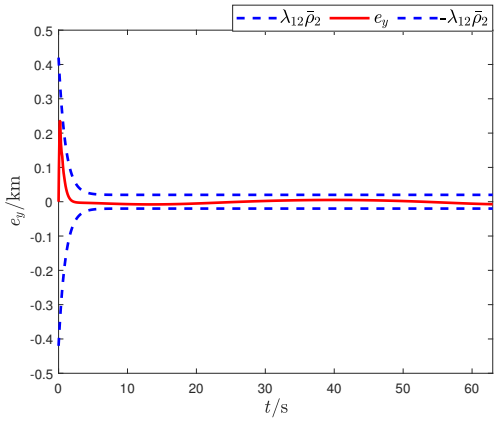

FIGURE 10 Error of e_y with precribed performance.

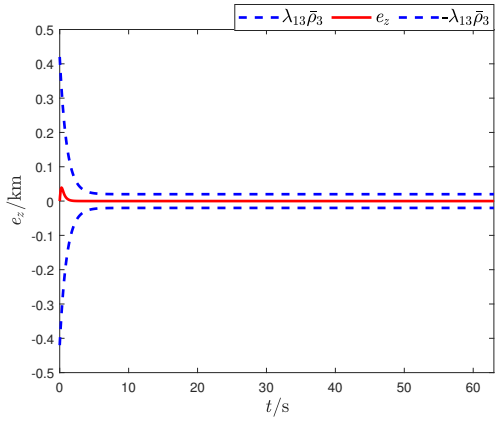

FIGURE 11 Error of e_z with precribed performance.

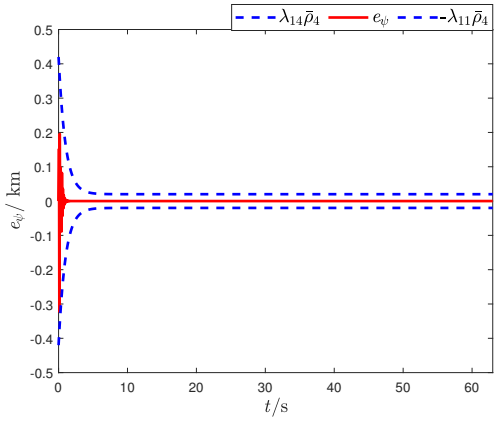

FIGURE 12 Error of e_ψ with precribed performance.

The final simulation results are presented in the Fig.7 -Fig.16 . Firstly, Fig.7 and Fig.8 demonstrate the effectiveness of the developed TTC method. The green and blue soild lines represent the actual output, and the desired input is represented by using the red dotted line. One can obtain that the actual output curve of the UAH can still track the planned three-dimensional space

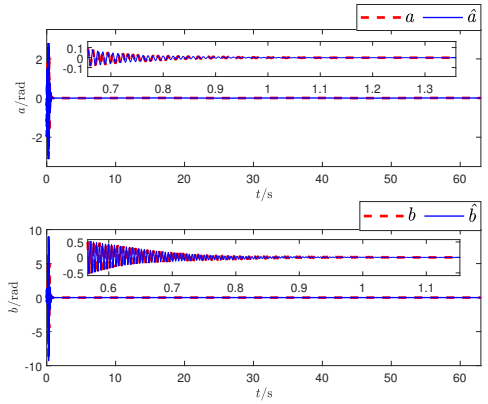

FIGURE 13 Estimation of unmeasurable states a and b.

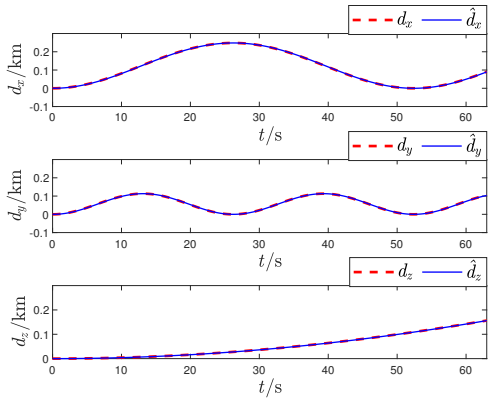

FIGURE 14 Tracking curves of ESO for disturbance D_P.

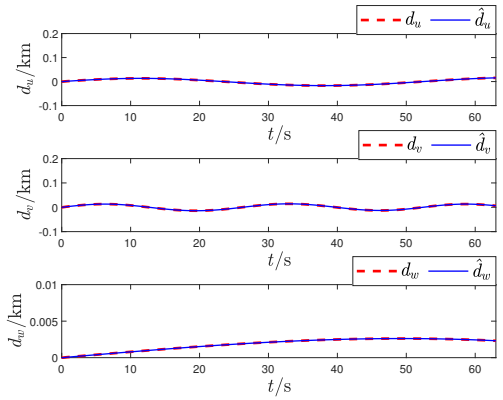

FIGURE 15 Tracking curves of ESO for disturbance D_V.

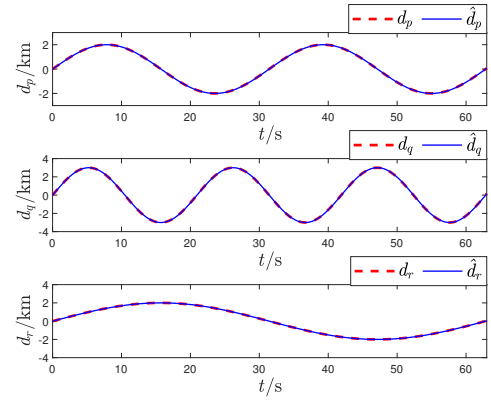

FIGURE 16 Tracking curves of ESO for disturbance D_Ω.

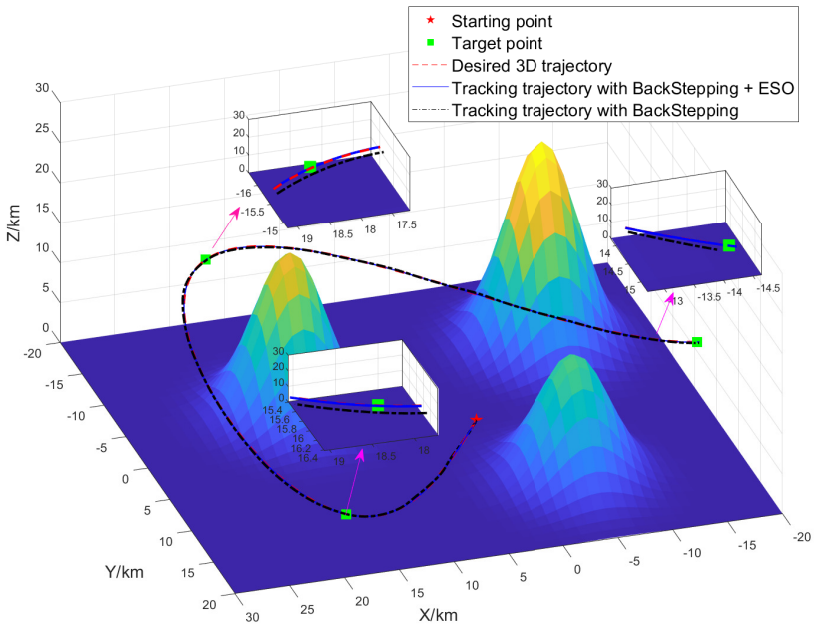

FIGURE 17 Diagram of 3D trajectory tracking comparision.

trajectory well in the present prescribed performance constraints and the external WGDs, which shows that the investigated TTC approach can ensure that the UAH has good tracking performance and stability.

Then, the Figs. 9 -12 present the output tracking error of the UAH under the prescribed performance constraints, which can be seen that by selecting valid control parameters, the output tracking error can be limited to the upper and lower bounds specified by the precribed performance function, so as to ensure the system achieves satisfactory control performance. In addition, the observation curve of the fractional-order observer and fractional-order ESOs for unmeasurable states and WGSs are shown in Figs. 13 -16 . We can observe that the designed fractional-order observers can quickly estimate the unmeasurable states a, b and the external WGDs, and the estimation errors are stable within a small range.

Moreover, to verify the effectiveness of the designed controller based on the fractional-order ESO in this paper, the proposed PMM-based control scheme is compared with the traditional backstepping control method without fractional-order ESO in the simulation of the tracking control, and the comparative simulation result is shown in Fig. 17 under the same control parameters. And based on Fig. 17 , it can be seen that the trajectory tracking control method proposed in this paper has better tracking effect. In conclusion, under the TTC method developed in this paper, the system of the UAH can achieve satisfactory tracking performance.

6 | CONCLUSION

In this paper, a backstepping TTC scheme based on the PPM is designed for the UAH with external WGDs and unmeasurable states. Firstly, the nonlinear model of a 6-DOF UAH under external WGDs has been established. Secondly, a fractional-order observer has been designed for unmeasurable states to estimate the flapping angles in actual flight. For the external disturbances, the fractional-order ESO has been designed. Then the controller of the trajectory tracking has been designed based on the backstepping method, and the tracking error is limited to the specified area through the PPM, which ensures the satisfactory performance of the tracking error. Then the stability of the entire system has been proved by constructing a Lyapunov function. Finally, the simulation results have demonstrated that the designed control approach can achieve the expected control objectives.

References

1. Yan K, Chen M, Wu Q. Neural network-based adaptive fault tolerant tracking control for unmanned autonomous helicopters with prescribed performance. *Proc Inst Mech Engrg, Part G: J Aerosp Eng* 2019; 233(12): 4350–4362.

2. Marantos P, Bechlioulis CP, Kyriakopoulos KJ. Robust trajectory tracking control for small-scale unmanned helicopters with model uncertainties. *IEEE Trans Control Syst Technol* 2017; 25(6): 2010–2021.

3. Xue S, Li Z, Yang L. Training a model-free reinforcement learning controller for a 3-degree-of-freedom helicopter under multiple constraints. *Meas Control* 2019; 52(7-8): 844–854.

4. Liu W, Chen M. An adaptive anti-swing control for the helicopter slung-load system based on trajectory planning and neural network. *Internat J Adapt Control Signal Process* 2022; 36(5): 1116–1140.

5. Rosales C, Soria CM, Rossomando FG. Identification and adaptive PID Control of a hexacopter UAV based on neural networks. *Internat J Adapt Control Signal Process* 2019; 33(1): 74–91.

6. Prempain E, Postlethwaite I. Static H_∞ loop shaping control of a fly-by-wire helicopter. *Automatica* 2005; 41(9): 1517–1528.

7. Zhang D, Duan H, Yang Y. Active disturbance rejection control for small unmanned helicopters via Levy flight-based pigeon-inspired optimization. *Aircraft Eng and Aerosp Technol* 2017; 89(6): 946–952.

8. Liu H, Lu G, Zhong Y. Robust LQR attitude control of a 3-DOF laboratory helicopter for aggressive maneuvers. *IEEE Trans Ind Electron* 2012; 60(10): 4627–4636.

9. Xian B, Jianchuan G, Yao Z, Bo Z. Sliding mode tracking control for miniature unmanned helicopters. *Chinese J Aeronaut* 2015; 28(1): 277–284.

10. Xian B, Guo J, Zhang Y. Adaptive backstepping tracking control of a 6-DOF unmanned helicopter. *IEEE/CAA J Automat Sin* 2015; 2(1): 19–24.

11. Shao S, Liu N, Li C, Chen M. Robust anti-swing control for unmanned helicopter slung-load system with prescribed performance. *Trans Nanjing Univ Aeronaut Astronaut* 2021; 38(2): 193–205.

12. Zou Y, Zheng Z. A robust adaptive RBFNN augmenting backstepping control approach for a model-scaled helicopter. *IEEE Trans Control Syst Technol* 2015; 23(6): 2344–2352.

13. Hu Y, Yang Y, Li S, Zhou Y. Fuzzy controller design of micro-unmanned helicopter relying on improved genetic optimization algorithm. *Aerosp Sci Technol* 2020; 98: 105685–1–12.

14. Lu H, Liu C, Guo L, Chen WH. Flight control design for small-scale helicopter using disturbance-observer-based backstepping. *J Guid Control Dyn* 2015; 38(11): 2235–2240.

15. Yu G, Cabecinhas D, Cunha R, Silvestre C. Nonlinear backstepping control of a quadrotor-slung load system. *IEEE/ASME Trans Mechatron* 2019; 24(5): 2304–2315.

16. Wang X, Yu X, Li S, Liu J. Composite block backstepping trajectory tracking control for disturbed unmanned helicopters. *Aerosp Sci Technol* 2019; 85: 386–398.

17. Wang X, Han L, Liu J. Attitude and height tracking control of unmanned helicopters with disturbances via disturbance observer-based composite dynamic surface control. *Trans Inst Meas Control* 2021; 43(14): 3294–3307.

18. Yan K, Chen M, Wu Q, Wang Y. Adaptive flight control for unmanned autonomous helicopter with external disturbance and actuator fault. *J Engrg* 2019; 2019(22): 8359–8364.

19. Xu LX, Ma HJ, Guo D, Xie AH, Song DL. Backstepping sliding-mode and cascade active disturbance rejection control for a quadrotor UAV. *IEEE/ASME Trans Mechatron* 2020; 25(6): 2743–2753.

20. Martini A, Léonard F, Abba G. Dynamic modelling and stability analysis of model-scale helicopters under wind gust. *J Intell Robot Syst* 2009; 54(4): 647–686.

21. Singh R, Bhushan B. Data-driven technique-based fault-tolerant control for pitch and yaw motion in unmanned helicopters. *IEEE Trans Instr Meas* 2020; 70: 3502711–1–11.

22. Yuksek B, Ure NK, Caliskan F, Inalhan G. Fault tolerant heading control system design for Turac unmanned aerial vehicle. *Trans Inst Meas Control* 2017; 39(3): 267–276.

23. Fang X, Liu F, Ding Z. Robust control of unmanned helicopters with high-order mismatched disturbances via disturbance-compensation-gain construction approach. *J Franklin Inst* 2018; 355(15): 7158–7177.

24. Li B, Hu Q, Yang Y. Continuous finite-time extended state observer based fault tolerant control for attitude stabilization. *Aerosp Sci Technol* 2019; 84: 204–213.

25. Wang N, Zhu Z, Qin H, Deng Z, Sun Y. Finite-time extended state observer-based exact tracking control of an unmanned surface vehicle. *Internat. J. Robust Nonlinear Control* 2021; 31(5): 1704–1719.

26. Li Y, Liu Y, Tong S. Observer-based neuro-adaptive optimized control of strict-feedback nonlinear systems with state constraints. *IEEE Trans Neural Netw Learn Syst* 2022; 33(7): 3131–3145.

27. Talole SE, Kolhe JP, Phadke SB. Extended-state-observer-based control of flexible-joint system with experimental validation. *IEEE Trans Ind Electron* 2009; 57(4): 1411–1419.

28. Li S, Yang J, Chen WH, Chen X. Generalized extended state observer based control for systems with mismatched uncertainties. *IEEE Trans Ind Electron* 2011; 59(12): 4792–4802.

29. Li Y, Min X, Tong S. Observer-based fuzzy adaptive inverse optimal output feedback control for uncertain nonlinear systems. *IEEE Trans Fuzzy Syst* 2020; 29(6): 1484–1495.

30. Chen Y, Petras I, Xue D. Fractional order control-a tutorial. In: IEEE 2009 American control conference. ; 2009: 1397–1411.

31. Xiao Y, Jin C. *The principle of flight in atmospheric distance*. National Defense Industry Press . 1993.

32. Kuo CW, Tsai CC, Lee CT. Intelligent leader-following consensus formation control using recurrent neural networks for small-size unmanned helicopters. *IEEE Trans Syst Man Cybern (Syst)* 2019; 51(2): 1288–1301.

33. Hou J, Chen M, Liu N. Unmanned helicopter control based on radial basis function neural network and extended state observer. *Control Theory Appl* 2021; 38(9): 1361–1371.

34. Léonard F, Martini A, Abba G. Robust nonlinear controls of model-scale helicopters under lateral and vertical wind gusts. *IEEE Trans Control Syst Technol* 2011; 20(1): 154–163.

35. Marconi L, Naldi R. Robust full degree-of-freedom tracking control of a helicopter. *Automatica*; 43(11): 1909–1920.

36. Chen M, Shi P, Lim CC. Adaptive neural fault-tolerant control of a 3-DOF model helicopter system. *IEEE Trans Syst Man Cybern (Syst)* 2015; 46(2): 260–270.

37. Aghababa MP. Design of a chatter-free terminal sliding mode controller for nonlinear fractional-order dynamical systems. *Int J Control* 2013; 86(10): 1744–1756.

38. Yang Y, Tan J, Yue D. Prescribed performance tracking control of a class of uncertain pure-feedback nonlinear systems with input saturation. *IEEE Trans Syst Man Cybern (Syst)* 2018; 50(5): 1733–1745.

39. Yan K, Chen M, Wu Q, Lu K. Robust attitude fault-tolerant control for unmanned autonomous helicopter with flapping dynamics and actuator faults. *Trans Inst Meas Control* 2019; 41(5): 1266–1277.

40. Yin C, Chen Y, Zhong Sm. Fractional-order sliding mode based extremum seeking control of a class of nonlinear systems. *Automatica* 2014; 50(12): 3173–3181.

41. Jinqiang H, Husheng W, Renjun Z, Rafik M, Xuanwu Z. Self-organized search-attack mission planning for UAV swarm based on wolf pack hunting behavior. *J Syst Eng Electronics* 2021; 32(6): 1463–1476.

42. Chen Y, Yang D, Yu J. Multi-UAV task assignment with parameter and time-sensitive uncertainties using modified two-part wolf pack search algorithm. *IEEE Trans Aerosp Electron Syst* 2018; 54(6): 2853–2872.

43. Liu Y, Li W, Wu H, Song W. Track planning for unmanned aerial vehicles based on wolf pack algorithm. *J Syst Simulation* 2015; 27(8): 1838.

44. Wang D, Huang J. Neural network-based adaptive dynamic surface control for a class of uncertain nonlinear systems in strict-feedback form. *IEEE Trans Neural Netw* 2005; 16(1): 195–202.

45. Chen M, Ge SS, Ren B. Adaptive tracking control of uncertain MIMO nonlinear systems with input constraints. *Automatica* 2011; 47(3): 452–465.

46. Li R, Chen M, Wu Q, Liu J. Robust adaptive tracking control for unmanned helicopter with constraints. *Int J Ad Robot Syst* 2017; 14(3): 1-12.

47. Roberge V, Tarbouchi M, LabontLabonté G. Comparison of parallel genetic algorithm and particle swarm optimization for real-time UAV path planning. *IEEE Trans Ind Inf* 2012; 9(1): 132–141.

48. Liu C, Liu A, Wang R, Zhao H, Lu Z. Path planning algorithm for multi-locomotion robot based on multi-objective genetic algorithm with elitist strategy. *Micromachines* 2022; 13(4): 616: 1-30.

49. Yan K, Chen M, Wu Q, Jiang B. Extended state observer-based sliding mode fault-tolerant control for unmanned autonomous helicopter with wind gusts. *IET Control Theory Appl* 2019; 13(10): 1500–1513.